



HAL
open science

One Martian Year of Near-Surface Temperatures at Jezero From MEDA Measurements on Mars2020/Perseverance

A. Manguira, R. Hueso, A. Sánchez-Lavega, D. Toledo, M. de la Torre Juárez,
A. Vicente-Retortillo, G. M. Martínez, T. Bertrand, T. del Rio-Gaztelurrutia,
E. Sebastián, et al.

► To cite this version:

A. Manguira, R. Hueso, A. Sánchez-Lavega, D. Toledo, M. de la Torre Juárez, et al.. One Martian Year of Near-Surface Temperatures at Jezero From MEDA Measurements on Mars2020/Perseverance. Journal of Geophysical Research: Planets, 2024, 129, 10.1029/2024JE008385 . insu-04853433v2

HAL Id: insu-04853433

<https://insu.hal.science/insu-04853433v2>

Submitted on 24 Dec 2024

HAL is a multi-disciplinary open access archive for the deposit and dissemination of scientific research documents, whether they are published or not. The documents may come from teaching and research institutions in France or abroad, or from public or private research centers.

L'archive ouverte pluridisciplinaire **HAL**, est destinée au dépôt et à la diffusion de documents scientifiques de niveau recherche, publiés ou non, émanant des établissements d'enseignement et de recherche français ou étrangers, des laboratoires publics ou privés.



Distributed under a Creative Commons Attribution - NonCommercial 4.0 International License

One Martian Year of Near-Surface Temperatures at Jezero From MEDA Measurements on Mars2020/Perseverance



Key Points:

- Seasonal variations in irradiance at Mars' surface drive observed daily mean near-surface air temperatures with some differences from models
- Thermal tides and long-period traveling waves present a clear seasonal cycle with autumn and winter seasons more prone to variability
- Air temperatures underwent non-seasonal changes near Jezero's delta, with strong daytime convection and nighttime gravity waves

Supporting Information:

Supporting Information may be found in the online version of this article.

Correspondence to:

A. Munguira,
asier.munguira@ehu.es

Citation:












Munguira, A., Hueso, R., Sánchez-Lavega, A., Toledo, D., de la Torre Juárez, M., Vicente-Retortillo, A., et al. (2024). One Martian Year of near-surface temperatures at Jezero from MEDA measurements on Mars2020/perseverance. *Journal of Geophysical Research: Planets*, 129, e2024JE008385. <https://doi.org/10.1029/2024JE008385>

Received 11 MAR 2024

Accepted 4 JUL 2024

Author Contributions:

Conceptualization: A. Munguira, R. Hueso, A. Sánchez-Lavega, D. Toledo, M. de la Torre Juárez, A. Vicente-Retortillo, G. M. Martínez, T. Bertrand, T. del Río-Gaztelurrutia, E. Sebastián, J. Pla-García
Data curation: M. de la Torre Juárez, E. Sebastián, J. A. Rodríguez-Manfredi
Formal analysis: A. Munguira, D. Toledo
Funding acquisition: R. Hueso, A. Sánchez-Lavega, M. de la Torre Juárez, J. A. Rodríguez-Manfredi
Investigation: A. Munguira

A. Munguira¹ , R. Hueso¹ , A. Sánchez-Lavega¹ , D. Toledo² , M. de la Torre Juárez³ , A. Vicente-Retortillo⁴ , G. M. Martínez⁵ , T. Bertrand⁶ , T. del Río-Gaztelurrutia¹ , E. Sebastián⁴, M. Lemmon⁷ , J. Pla-García⁴ , and J. A. Rodríguez-Manfredi⁴

¹Física Aplicada, Escuela de Ingeniería de Bilbao, Universidad del País Vasco UPV/EHU, Bilbao, Spain, ²Instituto Nacional de Técnica Aeroespacial (INTA), Madrid, Spain, ³Jet Propulsion Laboratory, California Institute of Technology, Pasadena, CA, USA, ⁴Centro de Astrobiología (CSIC-INTA), Madrid, Spain, ⁵Lunar and Planetary Institute (LPI), Houston, TX, USA, ⁶LESIA, Observatoire de Paris, Meudon, France, ⁷Space Science Institute, College Station, TX, USA

Abstract Measurements of ground and near surface atmospheric temperatures at Jezero obtained during 700 sols by the Mars Environmental Dynamics Analyzer (MEDA) characterize the thermal behavior of the near surface Martian atmosphere during a full Martian Year. The seasonal evolution of MEDA measurements is compared with predictions from the Mars Climate Database and the solar irradiance at the surface. Thermal tides observed in the daily cycle of temperatures follow a seasonal cycle with additional variations greater than 2 K on time-scales of tens of sols. We also observe sol-to-sol variations of about 1 K in mean daily air temperatures in autumn and winter with periodicities of 4–7 sols that might be related to baroclinic disturbances that are frequent in those seasons at high latitudes. We examine the evolution of the vertical thermal gradient and temperature fluctuations without finding a seasonal response to irradiance and dust load. We find that the convective boundary layer becomes isothermal and collapses 1 hr before sunset except during northern hemisphere winter, when the collapse occurs closer to sunset, implying a longer duration of the daytime convective instability. Around this period, the rover was located in the delta front in a location of complex topography where we observed stronger thermal gradients and intense daytime air temperature fluctuations. We also find in this place a nighttime event of gravity waves on near-surface air temperatures, with amplitudes of 2 K and periods of 10 min. These waves possibly propagate downward through a near isothermal stable layer.

Plain Language Summary The Perseverance rover on Mars is carrying a meteorological station that among other measurements obtains air temperatures at three heights near the surface as well as ground temperatures. We analyze seasonal and local changes in temperatures measured over one Martian year (687 Earth days) in which Perseverance moved several kilometers across Jezero crater, comparing in situ observations with the output from a Global Climate Model of the atmosphere of Mars. Our results show that the diurnal cycle of temperatures is modulated by the solar irradiance on the surface, the amount of dust in the atmosphere, local dynamics and large-scale weather systems. The temperature difference between the ground and the atmosphere greatly determines the meteorology in the lower atmosphere. Neither this temperature difference, nor temperature fluctuations, which during daytime are a proxy of atmospheric convection driven by the heating of the surface, show seasonal variations in line with the seasonal solar irradiance or dust load. Instead, the rover path toward a more complex topography led to the highest surface-to-air temperature difference during the northern hemisphere winter, despite the solar irradiance being minimum at that time. Close to this complex topography, the meteorological station recorded oscillations in near-surface temperature related to gravity waves.

1. Introduction

The Martian planetary boundary layer (PBL) is the lower part of the atmosphere that interacts with the surface. In the PBL, a variety of heat transfer and vertical mixing processes take place in a daily cycle that at large scales is modulated by seasons and locally by surface properties (Stull, 1988). In particular, differences between ground and near-surface air temperatures determine much of the daytime convective activity, and consequently, the strength of vertical mixing and the depth of the Convective Boundary Layer (CBL), which is the term commonly used to refer to the daytime PBL (Stull, 1988). Remote sensing measurements from orbit do not resolve the thermal gradient of the lowermost part of the PBL (Read et al., 2017), and in situ measurements with

© 2024 The Author(s).

This is an open access article under the terms of the [Creative Commons Attribution-NonCommercial License](https://creativecommons.org/licenses/by/4.0/), which permits use, distribution and reproduction in any medium, provided the original work is properly cited and is not used for commercial purposes.

Methodology: A. Munguira, R. Hueso, A. Sánchez-Lavega
Resources: A. Vicente-Retortillo, G. M. Martínez, T. Bertrand, T. del Río-Gaztelurrutia, E. Sebastián, M. Lemmon, J. Pla-García, J. A. Rodríguez-Manfredi
Software: A. Munguira
Supervision: R. Hueso, A. Sánchez-Lavega
Validation: A. Munguira, R. Hueso, M. de la Torre Juárez, E. Sebastián
Visualization: A. Munguira, R. Hueso
Writing – original draft: A. Munguira, R. Hueso
Writing – review & editing: A. Munguira, R. Hueso, A. Sánchez-Lavega

meteorological instruments are required to investigate this lower layer of the Martian atmosphere (e.g., Rodríguez-Manfredi et al., 2023). In situ measurements of temperature with a high cadence are sensitive to local processes such as turbulence and topographic flows. Temperatures are also affected by the atmospheric dust load, which varies on regional scales, and by other atmospheric processes occurring on global scales (e.g., thermal tides and other atmospheric waves). In addition, near surface atmospheric temperatures vary significantly from site to site (Martínez et al., 2017), and precise measurements of environment temperatures are relevant for validation of numerical models and for planning operations of landed missions (Kempenaar et al., 2018), including the future Mars Sample Return mission.

The Perseverance rover landed at Jezero crater (18.44°N, 77.45°E) on 18 February 2021. Among the different instruments carried on the rover, the Mars Environmental Dynamics Analyzer instrument (MEDA; Rodríguez-Manfredi et al., 2021a) is the meteorological package flown to study the Mars atmosphere at Jezero crater. MEDA contains several meteorological sensors including five Air Temperature Sensors (ATS) based on thermocouples and located at two altitudes above the ground—0.84 and 1.45 m—and Thermal InfraRed Sensors (TIRS), which measure the ground temperature and air temperature at around 40 m using infrared radiometry. The temperature measurements from these four levels improve our previous understanding of the thermal processes in the lower tens of meters of the atmosphere of Mars (Munguira et al., 2023; Rodríguez-Manfredi et al., 2023).

At present, MEDA observations around the clock span over more than a Martian Year (MY), which allows us to study the seasonal evolution of multiple quantities at both daytime and nighttime. Seasonal and latitudinal variations in solar irradiance are significant on Mars due to its axial tilt (25.2°) and orbit eccentricity ($e = 0.0934$). The atmospheric dust load also significantly affects the meteorology of Mars due to absorption of radiation at visible wavelengths and emission in the infrared (Read et al., 2015). The overall atmospheric dust load follows an annual cycle with slightly different features from orbit (Kass et al., 2016) and models and surface measurements (Figure 1a in Zurita-Zurita et al., 2022). This annual cycle is punctuated locally by the development of dust storms, and globally by a highly repetitive yearly cycle of dust abundance and by occasional global dust storms that develop in an unpredictable way (Kahre et al., 2017). The influence of these aspects on Martian air temperatures has been confirmed in several studies. For instance, Martínez et al. (2017) conducted a comprehensive review of in situ meteorological data collected from Mars, including temperature data, covering the landed missions on Mars from the Viking Landers (1970s) to the Curiosity rover in the Mars Science Laboratory (MSL) mission (landed in 2012 and still active). Recent surface missions such as Insight (Banfield et al., 2020) and Zhurong (Jiang et al., 2023) have also obtained air temperature measurements. Some of these missions have operated long enough to study the inter-annual variability at their specific locations (one Martian Year, MY, equals 687 Earth days). This is the case of Viking Landers (VL) 1 and 2 (Hess et al., 1977), Mars Exploration Rovers (Smith et al., 2004, 2006), the Curiosity rover (Gómez-Elvira et al., 2014) and the InSight lander (Banfield et al., 2020), with measurements from rovers being additionally affected by their paths over different terrains. Although most meteorological studies of seasonal and inter-annual variations on Mars have focused on the analysis of pressure data (e.g., Chatain et al., 2021; de la Torre Juárez et al., 2024; Hess et al., 1980; Ordoñez-Etxeberria et al., 2019), some recent studies also examine seasonal variations in temperature. For instance, Mason & Smith, (2021) used temperature records of 1,200 sols from the mini-TES radiometers in the Mars Exploration Rovers' (MERS) to investigate temperature fluctuations at different altitudes in the PBL (up to about 2 km), mostly during the day.

Munguira et al. (2023) presented a comprehensive study of near-surface temperatures at Jezero up to the Mars 2020 mission sol 400 (areocentric longitude, L_S , ranging 13–203°). That study presented a first characterization of the near surface air temperatures at Jezero and their role in PBL processes, together with an analysis of the performance of ATS and TIRS. Part of that analysis benefited from a comparison between temperature and wind data also measured by the MEDA instrument. However, the wind sensors on MEDA started to deteriorate around sol 313 (Viudez-Moreiras et al., 2022), and retrievals of wind data from measurements obtained by MEDA since then are not yet available. Here, we extend the analysis of MEDA temperature data up to mission sol 700 (L_S 21°, MY 37) covering a full Martian year. Temperature data from the second half of the MY 36 (L_S 180–360°) present more variability due to the combination of increased atmospheric dust load and dust variability (Kass et al., 2016), enhanced baroclinic activity over that part of the year (Barnes, 1980), and the path of the rover from the crater base to the delta front. The rest of this paper is structured in the following way: Section 2 describes the MEDA temperature data, summarizes the methodology used to take into account MEDA sampling gaps and also presents the rover's path along the mission. Section 3 studies the seasonal evolution of temperatures, including the

variability of daily mean temperatures during the second half of the MY 36. Section 4 reports changes in the daytime convective instability observed as the rover approached the delta. Section 5 presents the potential detection of gravity waves on near-surface temperatures close to the complex topography of the delta front. Finally, Section 6 summarizes the conclusions from this work.

2. Temperature Data

MEDA temperature data are most often recorded at 1 Hz, with some sols having temperature data sampled at 2 Hz, and are obtained simultaneously at four height levels (surface, 0.84, 1.45 m and at several tens of meters from infrared radiometry that is most sensitive to a 40 m height). The temperature data at 0.84 m were obtained by two ATS on the front of the rover. Environmental temperatures at 1.45 m were derived from measurements of three ATS located around the Remote Sensing Mast (RSM) of the rover. The location of these RSM sensors results in clean environment temperatures under most environmental conditions and less thermal contamination than in measurements obtained by the two ATS at the front of the rover (see Appendix B in Munguira et al., 2023). The thermocouples used in ATS have low thermal inertia and permit recording of fast temperature fluctuations at a sampling rate of 1 Hz (Pérez-Grande et al., 2017). This is also confirmed by comparisons with simultaneous air temperatures measured with the SuperCam microphone that is operated on a lower number of occasions but provides faster response on short periods of time (Chide et al., 2022). Surface temperature and air temperature from the first tens of meters of the atmosphere are measured by the Thermal Infrared Sensor (TIRS) using thermopiles sensitive to infrared fluxes (Rodríguez-Manfredi et al., 2021a). The air temperatures measured by TIRS were retrieved from the CO₂ spectral band at 15 μm. Due to the high optical depth of the atmosphere in this band, TIRS temperature measurements are effectively representative of the air temperature a few tens of meters above the surface (Smith et al., 2023), with a peak contribution from the atmosphere at around 40 m. This equivalent height varies slightly during a sol due to the diurnal evolution of the vertical thermal profile in the lower atmosphere, but the thermal gradient over that atmospheric layer is generally small. The accuracy of ATS temperatures and TIRS air temperatures are better than ±1 and ±3 K, respectively. The accuracy in the retrieval of the local surface temperature (representative of a small patch of terrain of 3 m²) is better than ±0.75 K, but the assumption of surface emissivity equal to one introduces additional uncertainties in this magnitude (Sebastián et al., 2020, 2021). Instrument noise levels of ~0.1 and ~0.45 K were reported for ATS and TIRS air temperatures, respectively, in Rodríguez-Manfredi et al. (2021a). These values correspond to nominal performance of the sensors at the beginning of the mission, while dust deposition events between sols 500 and 680 led to an increase in equivalent noise of ~0.13 K for TIRS temperature fluctuations near noon time.

This work focuses on the analysis of ATS temperatures at 1.45 m and TIRS air temperatures over the first tens of meters from the surface. Occasionally, we also present surface temperatures for context. ATS temperatures at 0.84 m are not presented to avoid additional difficulties in the interpretation of the data associated with the higher thermal contamination of these data. Measurements from the 3 ATS at 1.45 m are interpreted into a single measurement at each second using the procedure described in Munguira et al. (2023), which is basically a smooth adjustment to the ATS and returns the lowest measurements on a time-scale of a few minutes while preserving most of the thermal oscillations of that ATS.

2.1. Available Temperature Measurements

Figure 1 shows the temporal coverage of MEDA temperature data in Local True Solar Time (LTST) during the first 700 sols of mission operations. Since the landing of Perseverance, two main measurement cadences have been used to operate MEDA to monitor the diurnal cycle. The nominal cadence consists of taking measurements at even hours in even-numbered sols and at odd hours in odd-numbered sols, plus 5 min at the beginning of every other hour. This cadence covers over 55% of each sol and requires two sols to complete the diurnal cycle. However, around sols when Perseverance acquired samples of the Mars' terrain, that is, sampling sols, the MEDA cadence is generally limited to 15 min at the beginning of each hour due to power restrictions. Sampling related activities were frequent in the second half of MY 36 (e.g., sols 420–650 in Figure 1) as Perseverance approached the delta front.

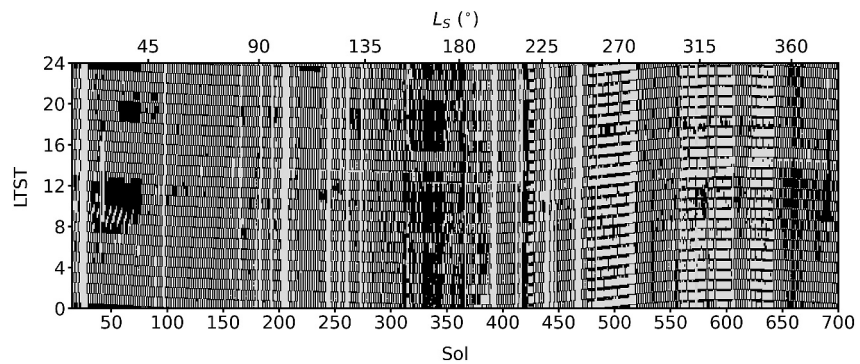


Figure 1. Mars environmental dynamics analyzer (MEDA) cadence of temperature measurements during the first 700 sols of Perseverance mission operations. Black squares indicate that meteorological records were taken at the corresponding Local True Solar Time and sol. Light-gray spaces indicate when MEDA was off. Solar longitudes are displayed on the upper x-axis.

2.2. Temperature Series Analysis

The uneven distribution of measurement blocks and gaps in the data require the use of fits to the observations to characterize the thermal evolution over each different sol. We used a Fourier series of daily data to study the diurnal cycle of temperature, removing the effect of small gaps and ignoring high-frequency oscillations in the recorded temperature data. The analysis consists of finding the Fourier series that best fits the daily temperature data, obtaining one Fourier series per sol for each altitude of interest. We tested Fourier series with 6–10 harmonics, but found that for sols with short measurement blocks of 15 min or less each hour the analysis was more stable with 6 harmonics. Results from 6 harmonics are almost indistinguishable from 10 harmonics in sols with larger amounts of temperature data, so we decided to use only six terms in the Fourier series. The use of 6 harmonics allows us to distinguish components of the thermal tides with periodicities in the range of 4–24 hr (see Munguira et al., 2023 for the specific mathematical description used here). Then, through visual inspection of the data and the fits we filtered out those sols where the parameters of the Fourier series are compromised due to large gaps in the data that do not allow to examine a full daily cycle, and/or discontinuities associated with rover drives in the case of the surface temperature.

Fourier analysis in Munguira et al. (2023) consisted in fitting the Fourier series to the combined temperature data of two consecutive sols as a function of LTST to fully cover a daily cycle with no gaps. Those fits do not resolve temperature changes that occur faster, for example, in one sol, but the alternate even-odd cadence, commonplace along the first 400 mission sols, resulted in robust fits with no significant loss of information (visual inspection of daily data shows little sol-to-sol variability on temperatures during the first half of MY 36). In contrast, temperatures during the second half of the MY (L_s 180–360°) are characterized by a larger sol-to-sol variability due to an increase in atmospheric dust load during the dusty season (Kahre et al., 2017) and enhanced seasonal baroclinic activity (Barnes, 1980). In addition, the MEDA cadence around sampling sols changed to 15 min at the beginning of each hour, leaving no reason to use data from two consecutive sols. Thus, in this work, we fit the temperature data of every single sol with Fourier series.

Figure 2 shows an example of the Fourier fits to temperature data in one sampling sol with only 15 min of data each hour. The diurnal cycle of temperature at each altitude is consistently represented by the resulting fit. Hence, fitting data from just one sol is typically enough to capture the overall shape of the temperature diurnal cycle, including daily maximum, mean and minimum temperatures.

2.3. Rover's Path Across Different Terrains

During the 700 sols analyzed in this work, the rover visited a diversity of terrains with different thermophysical properties (thermal inertia—TI—and albedo) and topographies. Figure 3 shows the landing site and posterior drive of Perseverance up to sol 708. The rover stayed close to the landing site for 379 sols, during which it conducted the *Jezero Crater Floor Science Campaign* after a first period of 100 sols of strategic operations (Sun et al., 2023). Between sols 379 and 410, the rover made a long drive toward the delta in the so-called *Rapid*

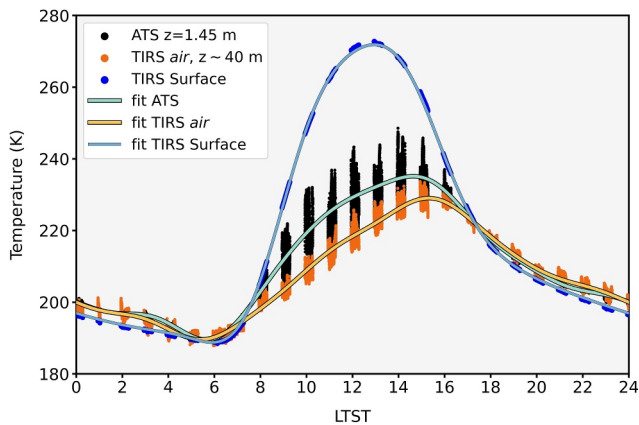


Figure 2. Fits of Fourier series to Mars environmental dynamics analyzer (MEDA) temperature data. Air temperature sensors and thermal infrared sensors data of sol 491 are marked as dots of different colors for each height (see legend), while color lines show the corresponding fits of the Fourier analysis at each altitude. On this sol, MEDA measured 15 min at the beginning of each hour as the Perseverance rover was saving power for sampling related activities.

Traverse Campaign. Thereafter, the rover explored the western delta front between sols 410 and 708 (*Delta Front Campaign*).

Terrain differences may cause changes in the local meteorology (Arya, 2001), particularly in sols in which the rover was close to the delta and exposed to different surfaces and different topographic driven winds from those found at the crater floor. Variations in local surface albedo and TI during the first 777 sols are presented in Martínez et al. (2024). Those results are calculated from MEDA data following the procedures described in detail in Martínez et al. (2023). The results show an increase in local surface albedo from roughly 0.12 to 0.18 and a slight decrease in TI from about 400 to $250 \text{ J m}^{-2} \text{ K}^{-1} \text{ s}^{-1/2}$ as Perseverance drove from the crater floor to the delta front. In addition to these variations in the thermophysical properties of the terrain, the new data analyzed in this work were obtained closer to the delta front than in Munguira et al. (2023), with potential meteorological effects related to the local topography discussed in Section 4 and Section 5.

3. Seasonal Evolution of Temperatures

In this section, we present the analyses of MEDA temperatures during a complete MY. An overview of the seasonal evolution of diurnal temperatures is presented in Section 3.1. Where possible, results are compared to meteorological predictions from the Mars Global Climate Model (Mars GCM) of the Laboratoire de Météorologie Dynamique (LMD). This model has been run over several Martian years and the output for each site, averaged as a function of L_S and LTST, is stored in the Mars Climate Database (MCD; Colaïtis et al., 2013; Forget et al., 1999; Millour et al., 2022). We used version 6.1 of MCD available at <https://www-mars.lmd.jussieu.fr/mars/access.html>.

ological predictions from the Mars Global Climate Model (Mars GCM) of the Laboratoire de Météorologie Dynamique (LMD). This model has been run over several Martian years and the output for each site, averaged as a function of L_S and LTST, is stored in the Mars Climate Database (MCD; Colaïtis et al., 2013; Forget et al., 1999; Millour et al., 2022). We used version 6.1 of MCD available at <https://www-mars.lmd.jussieu.fr/mars/access.html>.

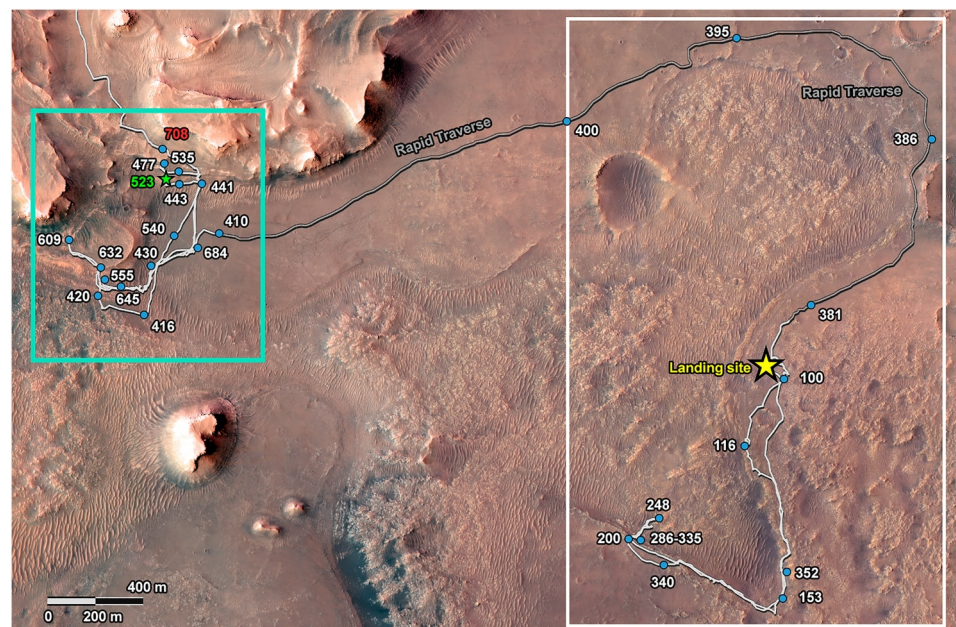


Figure 3. Perseverance's route during the first 708 sols of the Mars 2020 mission. The light-gray line indicates the route taken by the rover, with the dark-gray line highlighting the period of Rapid Traverse from the crater base floor to the delta front. The white square marks the rover's location during the first 400 sols of the mission, which was the period analyzed by Munguira et al. (2023). The turquoise square in the delta front shows where most of the new data analyzed in this work are concentrated. A yellow star pinpoints the rover's landing site. Blue dots and white numbers indicate the rover's stops on specific sols. The green star marks the location of the rover on sol 523 when the gravity wave event discussed in Section 5 was observed. The full trajectory of the rover since landing and an enlarged view of Jezero can be found at <https://mars.nasa.gov/mars2020/mission/where-is-the-rover/>.

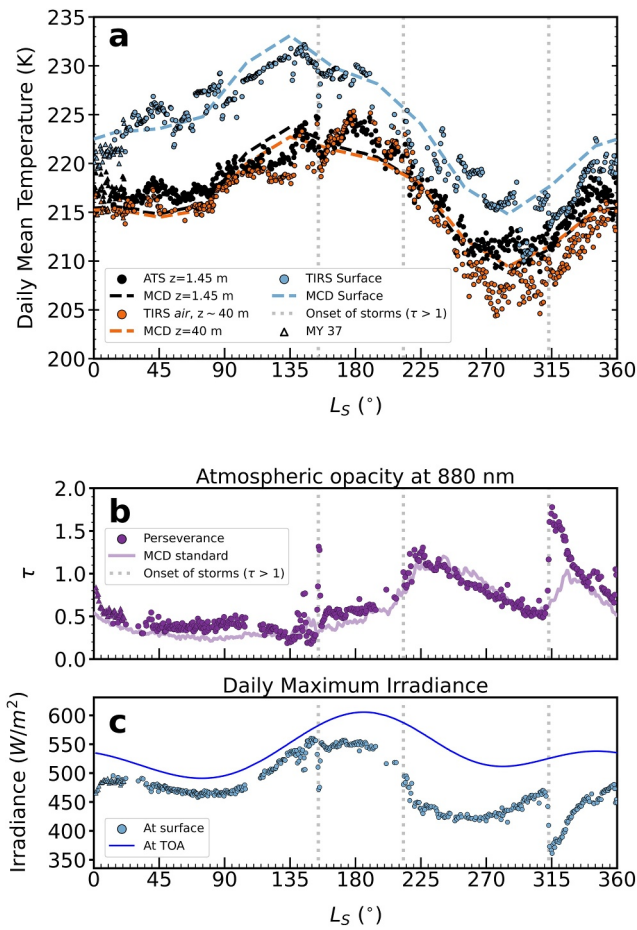


Figure 4. Seasonal evolution in near-surface temperatures at Jezero and main drivers of the evolution of temperatures as a function of L_S . (a) Seasonal evolution of mean daily temperatures at three altitudes (surface, 1.45 m and a few tens of meters). The colors for each height level are indicated in the legend of the figure. The Mars climate database (MCD) predictions are represented by the dashed lines in the same colors. Filled circles represent temperature data from MY 36, while temperature data from MY 37 are represented by triangles. (b) Atmospheric column opacity. Purple circles correspond to observational data from the MastCam-Z instrument at 880 nm, and the violet line shows the atmospheric column opacity considered in the standard climatology scenario from MCD. The times when atmospheric opacity exceeded $\tau > 1$ are marked by gray dotted lines in (a and b), highlighting the onset of storms at Jezero. (c) Daily maximum irradiance at the Top of the Atmosphere (TOA, dark blue line) and at the surface (light blue circles).

In this analysis, we considered the standard “climatology” dust scenario in which the GCM is run with a realistic seasonal distribution of dust (Lewis et al., 1999).

3.1. Daily Mean, Maximum and Minimum Temperatures

Figure 4 shows the daily mean temperatures at three altitudes (surface, 1.45 m and TIRS air temperature level) as a function of L_S . For each sol, daily mean temperatures were obtained from the constant term after fitting the temperature data with the Fourier series, as explained in Section 2.2. Daily mean temperatures at Jezero along MY 36 range from 210 to 232 K at the surface, 209–225 K at 1.45 m and 204 to 225 at the ~ 40 m level. The daily mean temperatures follow a seasonal cycle with annual amplitudes of 22 K, 16 and 21 K at these three levels, respectively (Figure 4a). The MCD predictions for daily mean temperatures roughly match the observations at Jezero. Some deviations between the MCD predicted values and observed temperatures are discussed later.

Figure 4b shows the atmospheric column opacity τ at a wavelength of 880 nm and as a function of L_S as retrieved from the analysis of light scattering effects in images obtained by the MastCam-Z instrument (Bell et al., 2022; Lemmon et al., 2022). The atmospheric column opacity at Jezero spans between 0.2 and 1.8 in MY 36. The opacity may increase either because of an increment of suspended dust or by the presence of water ice in the atmosphere. Three events indicated by vertical dashed lines in Figure 4b resulted in $\tau > 1.0$ and corresponded to the arrival of dust storms at Jezero. At $L_S 153^\circ$, a regional dust storm passed across Jezero, with this location being an active dust lifting location (Lemmon et al., 2022), while at $L_S \sim 213^\circ$ and $\sim 313^\circ$, the large A and C yearly storms (Kass et al., 2016) reached Jezero, respectively. In turn, clouds produced the greatest increase in the measured atmospheric opacity around $L_S \sim 145^\circ$, during the Aphelion Cloud Belt season (Patel et al., 2023; Smith et al., 2023; Toledo et al., 2023). This increase in atmospheric opacity was accompanied by an apparent increase in daily mean air temperatures (Figure 4a). The atmospheric opacity considered by the MCD (violet line in Figure 4b) as determined by Montabone et al. (2015) for the standard “climatology” dust scenario closely matches the observed atmospheric opacity at Jezero, although the model underestimates considerably the τ produced by the C storm, which is a consequence of the observed interannual variability associated with the C storm (Martín-Rubio et al., 2024).

Figure 4c shows the daily maximum solar irradiance at the Top of the Atmosphere (TOA) and at the surface as a function of L_S . These data are modeled following Vicente-Retortillo et al. (2015) and considering the orbital parameters of Mars, the rover location on the surface, and a radiative transfer code that models the solar irradiance at the surface from the TOA values and the measured atmospheric opacities shown in Figure 4b. For simplicity, the code assumes that the atmospheric column opacity retrieved from MastCam-Z images is solely caused by dust, since the effect of water ice clouds on solar irradiance arriving to the surface during daytime hours is minor in comparison (Martínez et al., 2017; Vicente-Retortillo et al., 2015). The irradiance at the surface is lower than at TOA because of the light that is scattered and absorbed by the particles in the atmosphere, causing notable dips in solar irradiance at the surface in the periods of high atmospheric opacity. We have found a notable linear correlation of daily mean atmospheric temperatures at 1.45 m with daily maximum irradiance at the surface ($r^2 = 0.72$). Similarly, the daily mean surface temperature in Figure 4a also correlates with the incoming solar irradiance at the surface, endorsing the importance of the radiative terms in the surface energy budget measured at Jezero (Martínez et al., 2023).

In general, daily mean temperatures in Figure 4a are greater at the surface than in the near-surface atmosphere due to the absorption of solar radiation by the ground during the daytime. However, after the onset of dust storms at Jezero crater (vertical gray lines in Figures 4a and 4b), the decline in solar irradiance at the surface (Figure 4c) results in a decrease in daily mean surface temperatures, which leads to a reduction in the surface-to-atmosphere temperature difference. Section 3.4 further explores the observed changes in atmospheric stability following dust storms. In contrast, the decrease in daily mean surface temperature around $L_S 300^\circ$ is not accompanied by a clear increase in opacity or by a reduction in atmospheric temperature. Hence, this decrease in surface temperature is likely explained by the change in the thermophysical properties of the local terrain found by Martínez et al. (2024) in that period. Note that Savijärvi et al. (2023), Rodríguez-Manfredi et al. (2023) and Munguira et al. (2023) showed that, while surface temperature varied considerably as the rover drove through terrains with different thermophysical properties, the atmospheric temperature seemed to be determined by the average surface properties of a wider terrain patch. This results in observations of some counter-intuitive effects, such as the break-up of nighttime inversions over small patches of terrain with unusually large values of the TI, and the high variability of surface temperatures observed in Figure 4a in particular groups of sols not being always accompanied by variations in ATS or TIRS air temperatures.

Figure 4a shows that daily mean atmospheric temperatures peak at $L_S 180^\circ$ while MCD temperatures peak at $L_S 135^\circ$. The observations agree better with multi-model simulations presented in Newman et al. (2021), where the maximum daily mean temperature is at $L_S 180^\circ$, also in agreement with the maximum solar irradiance at Jezero. In turn, the lowest daily mean temperatures occur at $L_S 280^\circ$ for the three height levels, in agreement with MCD predictions and the minimum irradiance at the surface excluding the period of the C storm. During the second half of MY 36, the sol-to-sol variability in daily mean atmospheric temperatures increased in both ATS and TIRS air temperature measurements. In this part of the Martian year, baroclinic wave activity becomes strong in northern mid-latitudes, with a peak of activity around the perihelion (Barnes, 1980; Lewis et al., 2016; Martínez et al., 2017). A quantitative analysis of atmospheric wave activity with periods above one sol that could be related to baroclinic activity is presented in Section 3.3.

One of the most puzzling differences between observations and MCD occurs during $L_S 270\text{--}300^\circ$. Daily mean temperatures at 1.45 m and the TIRS air level detach and separate from each other, implying a more intense thermal gradient in the near-surface atmosphere than expected from MCD predictions. Comparing these observed daily mean temperatures with MCD values, TIRS air temperatures are ~ 4 K colder, whereas temperature at 1.45 m is ~ 3 K warmer for no obvious reason. The opposite trends in ATS and TIRS may have implications for the near-surface meteorology; therefore, the following sections will devote some further discussion to the thermal environment observed during this period.

Figure 5 shows the evolution of daily maximum, mean and minimum temperatures at the surface, at 1.45 m and at the TIRS air temperature level and calculated via the Fourier analysis explained in Section 2.2. In MY 36, diurnal temperatures ranged from 183 to 266 K at 1.45 m (Figure 5a), 185–262 K at the first tens of meters sampled by TIRS (Figure 5b), and 178–290 K at the surface (Figure 5c). Overall, close to the surface, daily maximum temperatures are higher (due to the daytime solar absorption on the surface), while daily minimum temperatures are lower because of the efficient nighttime radiative cooling. In addition, daily minimum air temperatures vary considerably less than daily maximums over the year. At 1.45 m for example, the annual amplitude of daily minimum temperatures is only 16 K, while for maximum temperatures, they can vary by as much as 35 K with a peak in maximum temperatures of 266 K during the $L_S 135^\circ$ dust storm.

Surface temperatures in Figure 5c are colored as a function of the TI of the terrain retrieved as in Martínez et al. (2023). Changes in the TI of the terrain result in a large variability of local surface temperatures with a low impact on ATS temperatures and negligible impact on TIRS air temperatures (Munguira et al., 2023). Additional changes in surface temperatures are observed after the onset of dust storms (vertical dashed lines in Figure 5), which produce a nighttime warming and daytime cooling of the surface and atmosphere, as expected from the radiative properties of the dust and previous observations (e.g., Ryan & Henry, 1979). The only exception is the daytime atmospheric warming during the $L_S 153^\circ$ dust storm at Jezero attributed to the absorption of sunlight by low-altitude dust (Lemmon et al., 2022; Munguira et al., 2023).

MCD predictions are shown as black dashed lines in Figure 5 to illustrate whether departures between MCD predictions and observations are most important during daytime (with daily maximum temperatures as a proxy) or nighttime (daily minimum temperatures as proxy) at different times of the year. One of the most evident

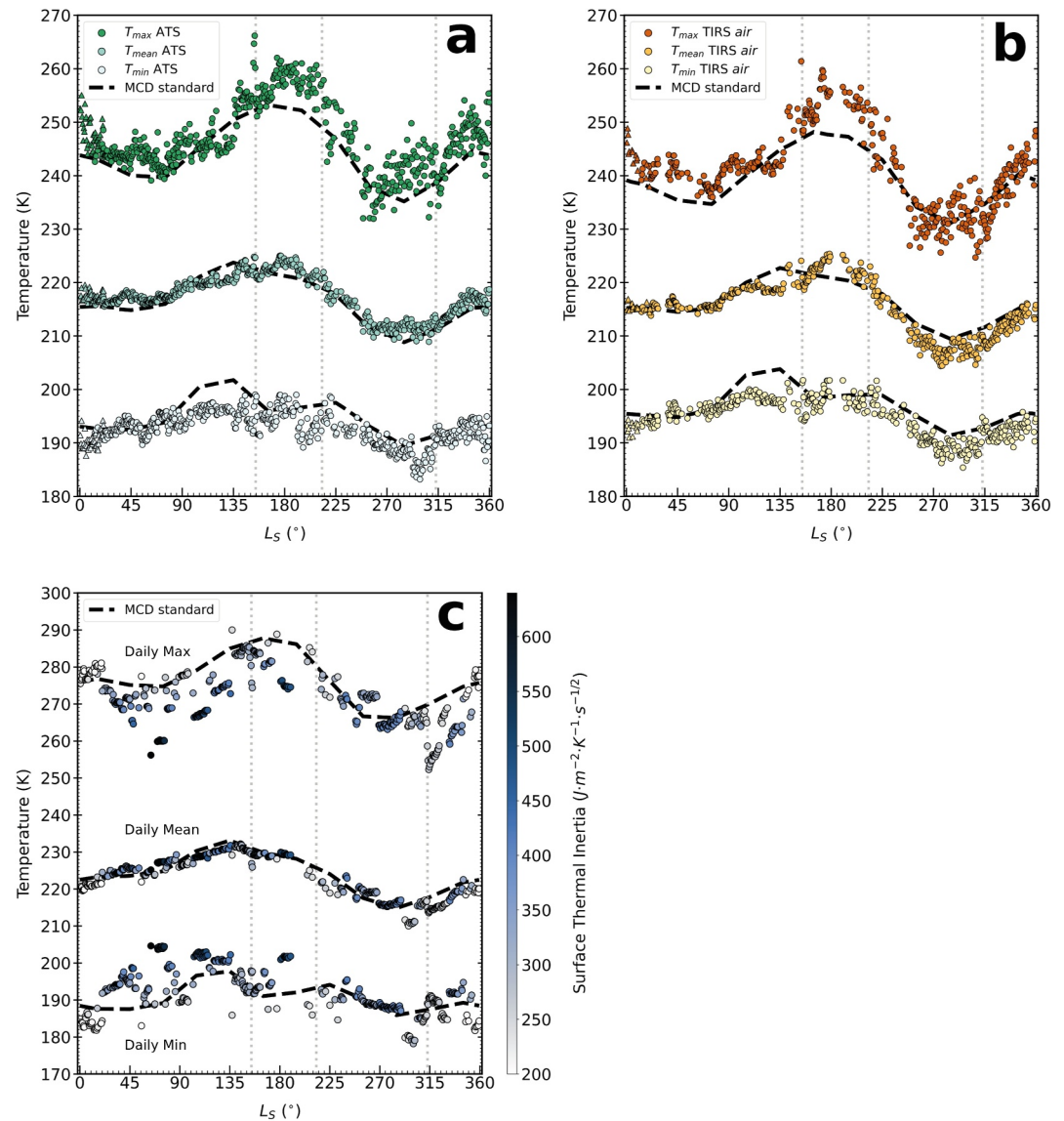


Figure 5. Diurnal maximum, mean and minimum temperatures from Mars environmental dynamics analyzer as a function of L_S . (a) Atmospheric temperature at 1.45 m from air temperature sensors, (b) atmospheric temperature at around 40 m (thermal infrared sensors (TIRS) atmospheric level) and (c) surface temperature retrieved with TIRS. In (a) and (b), different colors are used for maximum, mean and minimum temperatures (see legend); data for MY 36 are represented with filled circles, while data from MY 37 are represented with triangles. Note that the vertical scale is different in (c). Colors in (c) correspond to the local surface thermal inertia for each sol and L_S following Martínez et al. (2023, 2024). Predictions from the standard climatology scenario of the Mars climate database are shown as dashed black lines. The onset of dust storms at Jezero is indicated by vertical dotted lines as in Figure 4.

differences between MEDA and MCD is the difference of ~ 10 K between both in daily maximum atmospheric temperatures centered around $L_S 180^\circ$ and occurring at the time of maximum solar irradiance (Figure 4c). The higher amount of dust ($\tau = 0.6$ at $L_S 160\text{--}210^\circ$ in Figure 4b), if produced mainly by dust present at low altitudes, might be enough to explain the difference. In addition, Figures 5a and 5b show that MCD overestimates minimum atmospheric temperatures between $L_S 90\text{--}150^\circ$ by ~ 5 K, while maximum temperatures match reasonably well with the observations at this time. Numerical models discussed by Newman et al. (2021) attributed the anomalous high minimum temperatures in MCD to the effect of water ice clouds, which would emit downward longwave radiation at nighttime, reducing the nighttime cooling, while their effect would be negligible on daytime temperatures. In addition to that, modeled near-surface temperatures depend on the parameterization of turbulence

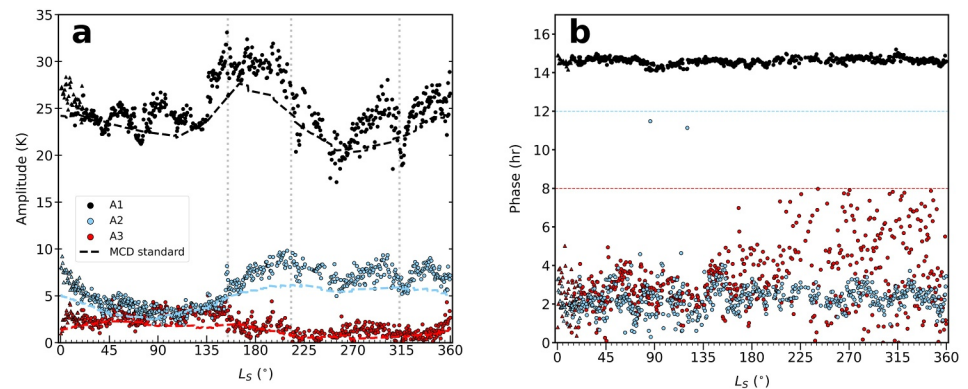


Figure 6. Seasonal evolution of thermal tides from near-surface temperature data at 1.45 m. (a) Amplitudes of the first three modes of the thermal tides as a function of L_S (see colors in the legend of the figure). Vertical dotted lines indicate the onset of storms at Jezero, as shown in Figure 4. Dashed lines correspond to Mars climate database predictions. (b) Phases (in local true solar time) of the first three modes of the thermal tides as a function of L_S . Blue and red horizontal dashed lines indicate the limit to the maximum phases of the semidiurnal (12-hr periodicity) and terdiurnal (8-hr periodicity) modes, respectively.

and near-surface fluxes in atmospheric models (e.g., using Monin-Obukhov similarity theory). Under stable nocturnal conditions, these parameterizations are often problematic for Mars and even for the Earth (Cheng et al., 2005; Read et al., 2017), and the 5 K mismatch between MCD and MEDA night-time temperatures could be related to these difficulties experienced by models under nocturnal conditions.

During L_S 270–300°, temperatures at the three levels and their departures with respect to MCD cannot be fully explained by the atmospheric dust opacity or by albedo or TI changes. In particular, we note the increase in maximum temperatures at 1.45 m during the northern hemisphere winter, when temperatures typically drop to their minimum values. If we compare MEDA observations with MCD, daily maximum temperatures at 1.45 m were ~5 K higher on average (and up to 15 K higher on some individual sols), while TIRS daily maximum temperatures oscillated around predicted values. On the other hand, minimum ATS temperatures at 1.45 m did not show a consistent increase/decrease throughout the period. The fact that MCD is unable to explain these ATS observations probably implies that the changes in temperatures occur locally rather than globally. In Section 4, we examine the possible effects on the meteorology associated with the topography near the delta.

3.2. Seasonal Evolution of Thermal Tides

Thermal tides are planetary scale phenomena that propagate in the Martian atmosphere in response to the diurnal solar irradiance (Leovy, 1977). The amplitude and phase of the tides are modulated by seasonal irradiance, atmospheric dust and cloud content, and regional surface properties and topography. The contribution of the atmospheric tides to the near-surface meteorology is typically studied through Fourier analysis of surface pressure data (e.g., Guzewich et al., 2016; Leovy & Zurek, 1979; Sánchez-Lavega, del Río-Gaztelurrutia, et al., 2023). Munguira et al. (2023) showed that MEDA's ATS accuracy and temporal coverage also enable the study of thermal tide components from near-surface temperature data. Here, we analyze the seasonal variation of the modes that contribute the most to shaping the diurnal cycles of temperatures at 1.45 m. Figure 6 shows the amplitudes and phases of the diurnal, semidiurnal and terdiurnal modes of the thermal tides as a function of L_S . We do not include higher order modes because their amplitudes are residual. The same Fourier analysis is performed over MCD data and is included in Figure 6a (dashed lines) to help in the interpretation of the tides.

The diurnal mode contributes by far the largest amplitude (~25 K) to near-surface temperature (Figure 6a), since temperatures rise notably once every sol following the rotation of the planet and consequent solar irradiance cycle. This mode also has a nearly constant phase, which is a consequence of the highly repetitive shape of the diurnal temperature cycle near the surface. Overall, the diurnal mode follows the seasonal cycle of solar irradiance. For example, around the northern fall equinox (L_S 180°), the diurnal mode presents a notable increase, both in observed behavior and MCD data, that coincides with the maximum irradiance at the TOA (Figure 4c) above Jezero.

The amplitudes of the semidiurnal and terdiurnal modes in Figure 6a are responsible of the asymmetry in the shape of the diurnal temperature cycle and evolve considerably during a full Martian Year. Both components have similar amplitudes during the Aphelion Cloud Belt season (L_S 45–150°), which correspond to a period of nearly constant irradiance and atmospheric opacity (Figures 4b and 4c). The dustier period of the MY starts around L_S 150° and extends to L_S 360°, when a great amount of dust is injected into the atmosphere and spreads over planetary scales. This period produces opposing effects in the amplitudes of the semidiurnal and terdiurnal modes. While the amplitude of the semidiurnal mode doubles, the amplitude of the terdiurnal mode drops to the noise level and consequently its phase becomes chaotic (Figure 6b), meaning that the contribution of the terdiurnal tide is residual after L_S 150°. Otherwise, the phases of the three modes in Figure 6b are largely uniform during the whole MY.

The diurnal and semidiurnal tides in temperature show an increase in their amplitude during the onset of the local dust storm at L_S 150°. They also show a reduction in amplitude during the sharp changes in dust content associated with the A and C storms at L_S ~213° and ~313° respectively. Although diurnal and semidiurnal tides do react to dust storms, these effects are still very small compared to the stronger variations in the atmospheric tides in pressure (Guzewich et al., 2016; Sánchez-Lavega, del Rio-Gaztelurrutia, et al., 2023), and suggest a low influence of the global dynamics on near surface temperatures.

In addition to the seasonal variations in irradiance and dust load, the amplitude of the diurnal mode also oscillates in sub-seasonal time scales. Figure 7a shows the diurnal mode amplitude compared with the solar irradiance at TOA and at the surface over an entire MY. Although seasonal effects are clear in this amplitude, there are additional oscillations that are not explained by variations in the solar irradiance at the surface. These oscillations are notable around L_S 45–100° and L_S 270–315°, and are probably representing variability on time-scales of tens of sol caused by variations in the cloud optical depth (Smith et al., 2023) and atmospheric dynamics. Battalio et al. (2022) and Munguira et al. (2023) discussed the possibility that atmospheric waves could be causing the temperature variations identified before L_S 150°. To quantify the magnitude of the oscillations, we fitted the diurnal mode amplitude over the MY to a sine function (the best fit is given by the black line in Figure 7a). Figure 7b shows the oscillations in the amplitude of the diurnal mode after subtracting the fit and it suggests oscillations of 3–5 K with periods of tens of sols. While some of these variations seem correlated with variations in dust opacity and irradiance at the surface, particularly during the L_S 153° dust storm and A and C storms, most of these changes seem uncorrelated with dust activity. The fact that these variations seem uncorrelated with variations in surface pressure measured by MEDA and presented by Sánchez-Lavega, del Rio-Gaztelurrutia, et al. (2023) does not allow us to further investigate the source of these variations.

3.3. Long-Period Traveling Waves

Periodic variations in daily mean temperatures with amplitudes of about 1 K have been observed at Jezero on MEDA temperature data (Battalio et al., 2022, Munguira et al. 2023). These variations have been proposed to be caused by the arrival of large-scale atmospheric waves originating from baroclinic activity at higher latitudes (Barnes, 1980, 1981, 1984). Pressure data have shown similar regular oscillations with periods above one sol superimposed over the seasonal evolution of pressure at a wide range of Martian locations (Banfield et al., 2020; Barnes, 1980; Haberle et al., 2018) including Jezero (Sánchez-Lavega, del Rio-Gaztelurrutia, et al., 2023). However, as Barnes (1980) found in the Viking Lander 2 data set, the oscillations in the local temperature and pressure fields are not directly correlated.

To quantify the amplitudes of the atmospheric waves, we fitted and subtracted a second-order polynomial to the daily mean temperatures at 1.45 m presented in Section 3.1. We subdivided the data of daily mean temperatures into groups of continuous data and fit those continuous sets in intervals of 20 consecutive sols disregarding periods with no continuous data on that time-scale. For intervals before L_S 90° and between L_S 180 and 250° fits were calculated using intervals of only 10 consecutive sols due to the more frequent discontinuities in the data produced by rover activities. Intervals of 10–20 sols retain the contribution from waves with periods of 3–4 sols and reduce artifacts at small frequencies of several tens of sols associated with the seasonal variation of temperature.

Figure 8a presents the results of that analysis for MEDA air temperature data and shows low amplitudes of ± 0.25 –0.5 K for temperature oscillations between L_S 20 and 120°. This “quiet” period corresponds to the aphelion season of MY 36 that presented a steady solar irradiance at the surface (Figure 4c) and the lowest atmospheric wave

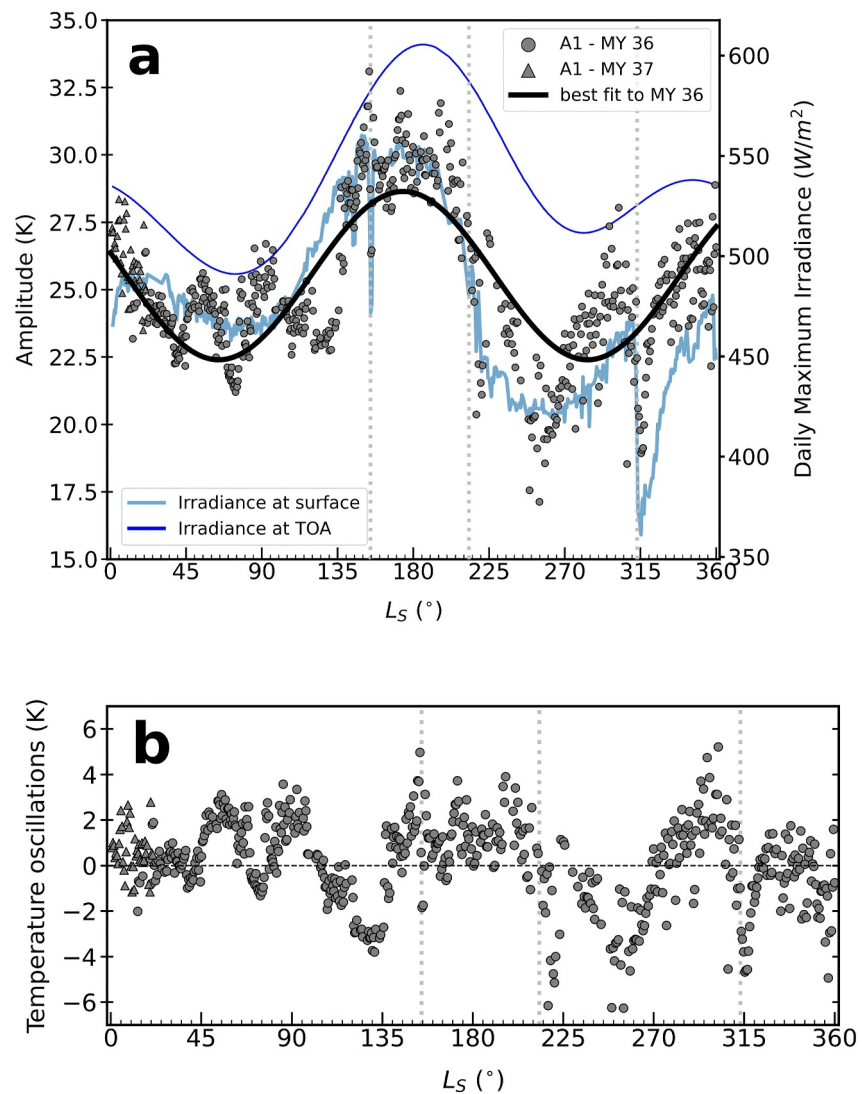


Figure 7. Oscillations in the diurnal tide on sub-seasonal timescales. (a) Diurnal mode amplitudes as a function of L_S (gray circles) compared with the solar irradiance at the surface and at top of the atmosphere (TOA) (see legend). The black line shows the best fit of the diurnal mode to a sine function, which has phase and frequency comparable to the seasonal irradiance at TOA. (b) Oscillations in the diurnal mode with respect to its best fit. Vertical dotted lines indicate the onset of storms at Jezero.

activity. We used this period to determine the noise level of the daily mean temperature oscillations (horizontal dashed lines in Figure 8a), that is, the minimum amplitude that is significant regarding sol-to-sol variability in the MEDA data set. The standard deviation of the temperature oscillations through the quiet period up to sol 110 gives an estimation of 0.3 K in the noise level associated with the sol-to-sol variation of mean temperatures. The strong variations during the L_S 153 $^\circ$ dust storm appear clearly in the analysis in Figure 8a, with sol-to-sol variations in temperatures of up to 2 K, but the analysis is inconclusive about short-term variations associated with the arrival of storms A and C. However, during the northern hemisphere autumn and winter, sol-to-sol temperature variations intensified, especially after L_S 300 $^\circ$, and reached amplitudes of ± 1.5 K in the temperatures at 1.45 m above the surface. However, the winter solstice (L_S 270 $^\circ$) presents relatively low temperature oscillations, in agreement with the solsticial pause reported by Wang et al. (2005) and Lewis et al. (2016).

Figure 8b shows oscillations in daily mean temperatures predicted by the GCM on which the MCD is based. The way in which MCD implements large-scale perturbations is explained in Lewis et al. (1999) and Millour et al. (2017), and summarized in Manguira et al. (2023). Briefly, the variability obtained on GCM simulations is

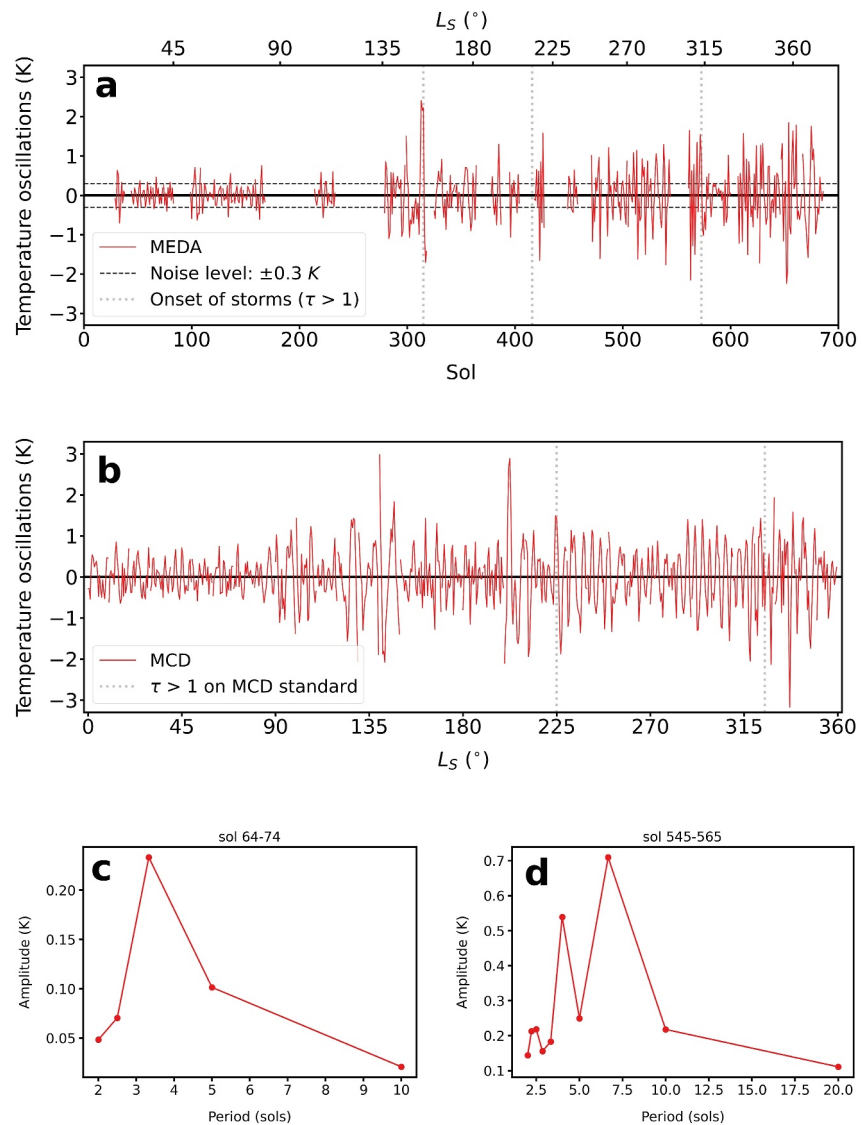


Figure 8. Atmospheric waves with periods above one sol detected at 1.45 m in Jezero crater. (a) Oscillations of daily mean temperatures from MEDA's air temperature sensors at 1.45 m as a function of sol and L_S . Vertical dotted lines indicate the onset of dust storms at Jezero. Horizontal dashed lines correspond to the estimated noise level of ± 0.3 K (see text) (b) Oscillations of daily mean temperatures predicted by Mars climate database at 1.45 m during all solar longitudes. Vertical dotted lines indicate the predicted onset of *A* and *C* dust storms at Jezero under the standard dust climatology scenario. (c) and (d) show the amplitudes and periods of the temperature variations shown in (a) between sols 64–74 and 545–565, respectively, with results in (c) being inconclusive and below the noise error of this analysis.

synthesized on Empirical Orthogonal Functions for each of its output variables. This allows us to add the representative variability of the original GCM simulations to the MCD smooth behavior. The analysis of temperature variations in Figure 8b uses running windows of 10° in L_S (roughly corresponding to 20 sols and moving smoothly in steps of 0.5° or 1 sol) to analyze oscillations in MCD air temperature data. The analysis of the variability on the MCD data generally agrees with the results of our analysis of the MEDA data. Together they suggest that oscillations of near-surface temperatures of ± 0.5 K before L_S 90° grow to variations of ± 1 – 2 K after L_S 270° , and that most of these variations are not associated with the motion of the rover but with seasonal variability.

To analyze the periods of the atmospheric waves detected with ATS, Figures 8c and 8d present periodograms for two fragments of detrended mean air temperature data in Figure 8a (sols 64–74 and sols 545–565). These two groups of sols are representative of the times of the year with the lowest and highest contributions from

atmospheric waves to near-surface temperatures, respectively. Short and inconclusive periodicities of about 3 sols are found in the quiet period represented by sols 64–74, where the amplitudes of these oscillations are below the 0.3 K noise level assumed for the analysis. However, atmospheric waves with periods of 4–7 sols and robust amplitudes of 0.5–0.7 K dominate in the variable active period represented by sols 545–565. Comparing Figures 8a and 8b, the periods (peak-to-peak) involved in MCD data seem slightly higher, but we attribute this to the fact that MCD uses interpolation methods to provide meteorological variables on a daily basis.

In addition, we further examine our results in temperature by comparing them with published analysis of surface pressure data. Sánchez-Lavega, del Río-Gaztelurrutia, et al. (2023) and Sánchez-Lavega, Larsen, et al. (2023) analyzed MEDA pressure data and reported low wave amplitudes before L_S 130° with a posterior intensification of pressure oscillations, and strong disturbances in pressure at the onset of the important dust storms at Jezero. Atmospheric waves with periods between 3 and 10 sols seemed to dominate the daily pressure oscillations. In addition, maximum wave contributions to surface pressure also took place after L_S 270° on MY 36 (Sánchez-Lavega, Larsen, et al., 2023). Overall, there is a good agreement between the time of the MY in which MEDA observed the strongest variability in daily mean temperatures and daily mean pressures, although the observed frequencies associated with these variations are only approximately similar. The major difference between variations in pressure and temperature is that we do not observe significant disturbances in near-surface temperatures coinciding with the onset of A and C storms at Jezero, when clear variations in pressure were identified in analyses of pressure data by Sánchez-Lavega, Larsen, et al. (2023). The strongest disturbance of ± 2 K in Figure 8a occurred during the regional dust storm that covered Jezero at L_S 153°, and was possibly due to the local dust lifting processes and variations in the heating of the atmosphere and surface that took place locally (Lemmon et al., 2022), without the need to imply atmospheric waves to explain these temperature variations. Finally, the apparent activity of atmospheric waves in near surface air temperature was significantly reduced for almost 30 sols after the arrival of the C storm at Jezero, possibly due to the vertical homogenization of the atmosphere induced by atmospheric dust. This confirms the interpretation of the local response in temperature that was observed at Viking landers locations after dust storms (Ryan & Henry, 1979). Similarly, Barnes (1980) observed an important reduction in the amplitude of pressure oscillations at the Viking Lander 2 location (48°N) following the onset of a large dust storm.

3.4. Temperature Fluctuations and Atmospheric Stability as a Function of LTST and L_S

A capability unique to MEDA is its ability to measure thermal gradients near the Martian surface. Rodríguez-Manfredi et al. (2023) showed how temperature fluctuations and thermal gradients measured by MEDA can characterize the turbulence in the CBL in Jezero. De la Torre Juárez et al. (2023) further analyzed the statistical properties of fluctuations of MEDA winds and temperatures on selected sols to find different turbulence regimes in the near surface atmosphere, and Manguira et al. (2023) quantified the thermal oscillations over 400 sols as a proxy of the varying level of daytime near-surface convective activity at Jezero, finding a linear relation between temperature fluctuations and thermal gradients during daytime. An additional analysis by Pla-García et al. (2023) concluded that topographic flows driving turbulence during nighttime also cause temperature fluctuations.

Here we quantify temperature fluctuations and vertical thermal gradients from MEDA data, extending the results presented in Manguira et al. (2023). The period from L_S 5–20°, low in atmospheric dust, is available for both MY36 and MY37 and constitutes a valuable proxy to assess if annual repeatability is present in temperature fluctuations and thermal gradients. We first averaged MEDA temperature data in 5-min windows. This window length is long enough to capture a significant sample of temperature records, allowing for the characterization of statistical properties such as mean temperature and standard deviation. At the same time, 5 min is short enough to exclude variations in the level of fluctuations associated with the diurnal cycle of temperatures, which at some critical times of the daily cycle such as sunrise can modify temperature fluctuations on time-scales as short as 15 min. In addition, in each of the 5-min windows, temperature fluctuations are evaluated after subtracting a second-order polynomial fit to each 5-min window, which effectively removes any remaining diurnal evolution of mean temperatures. The standard deviation σ_T of the detrended temperatures in these 5-min windows is used as a measurement of the intensity of the temperature fluctuations. In addition, thermal gradients from the difference between mean temperatures observed at different heights by MEDA are determined using the same time scale of 5 min.

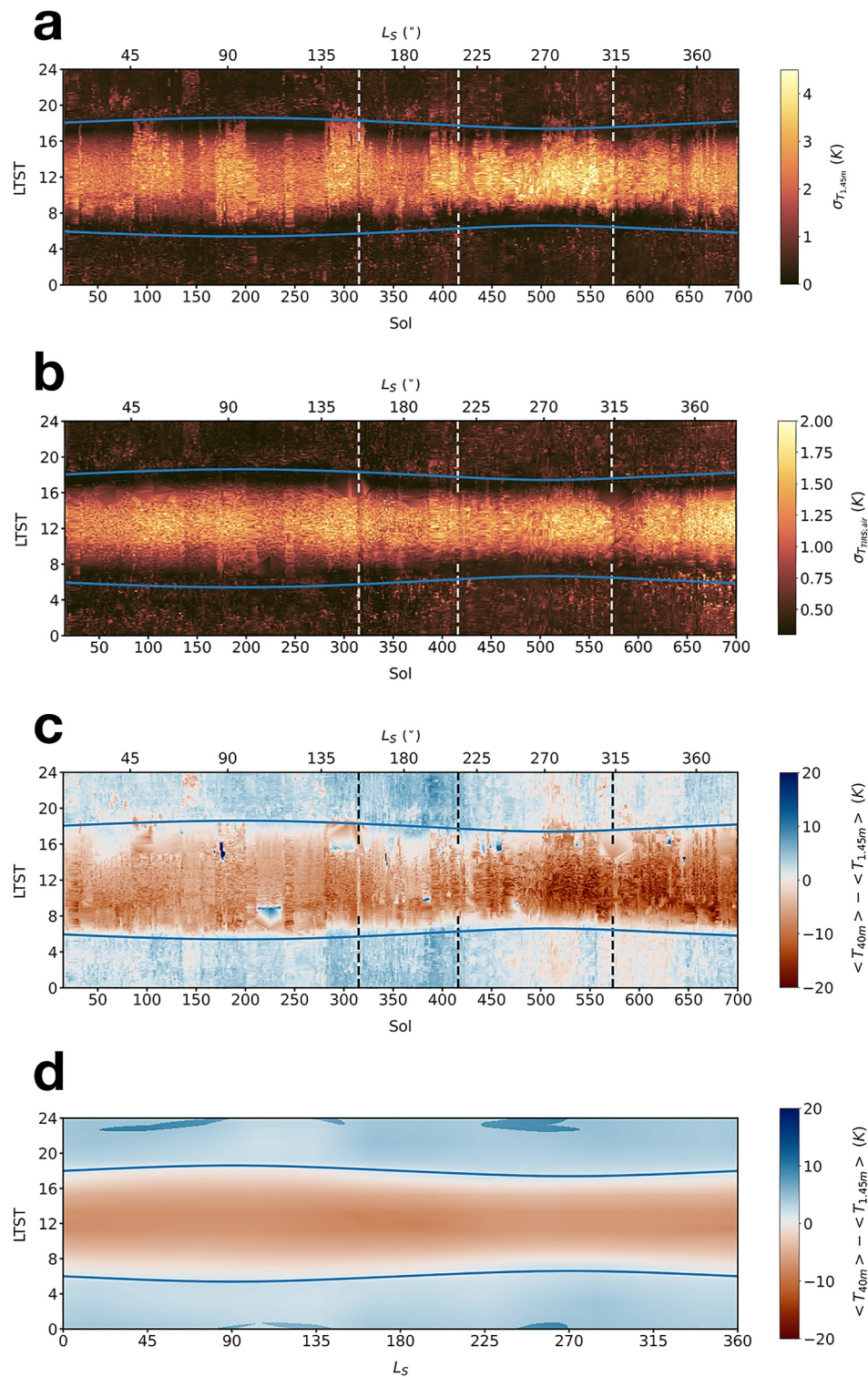


Figure 9. Evolution of temperature fluctuations and atmospheric stability as a function of local true solar time (LTST) and sol/ L_S . (a) Standard deviations of high-frequency temperature fluctuations at 1.45 m in 5 min windows. (b) Standard deviations of high-frequency thermal infrared sensors (TIRS) air temperature fluctuations in 5 min windows. (c) Difference between mean temperatures at TIRS air temperature level and at 1.45 m in 5 min windows. A triangular interpolation in L_S and LTST is used in (a–c) to mask gaps in temporal coverage. Some artifacts arise in (b and c) since TIRS data are discarded when the Sun at an elevation of 35° enters the FoV of the sensor's upward-looking channel. (d) Difference between atmospheric temperatures at 40 and 1.45 m for the Mars Climate Database predictions with a cadence of 5 min. Blue lines indicate the times of sunrise and sunset. Vertical dashed lines in (a–c) indicate the onset of dust storms at Jezero.

Temperature fluctuations at 1.45 m and at the TIRS air temperature level are shown as a function of LTST and L_S in Figures 9a and 9b. The near-surface thermal gradient of the atmosphere is also shown as a function of LTST and L_S in Figure 9c from the difference between 5-min averages of ATS temperature at 1.45 m and TIRS air temperature. This vertical temperature difference determines the atmospheric vertical stability. The near-surface atmosphere is convective if the temperature difference is negative, and is stably stratified otherwise. Note that in this analysis we do not use the surface temperature since this magnitude varies strongly depending on the value of the TI of the local terrain, which can be very different from sol to sol due to the presence of large and small patches of the terrain with anomalous values of TI. Thus, surface temperatures produce discontinuities in the local thermal gradient that are not replicated when examining the thermal gradient from the 1.45 and 40 m levels (Munguira et al., 2023). For comparison, the thermal gradient calculated from MCD data (MCD temperature extrapolated at 40 m minus MCD temperature extrapolated at 1.45 m) is displayed in Figure 9d, showing that in general the overall evolution of the thermal gradient from MEDA data and MCD predictions are in good agreement.

Temperature fluctuations in Figures 9a and 9b do not show clear seasonal trends during the first Martian Year of observations (MY 36). Discontinuities in diurnal temperature fluctuations observed around sols 100, 200 and 300 in Figure 9a are associated with eastward-westward rover orientations that partially influence ATS temperature measurements. Variations in the surface thermophysical properties of the terrain only add minor variations in ATS measurements (Munguira et al., 2023). The air temperature fluctuations recorded by TIRS and shown in Figure 9b are not subject to the thermal effects associated with the rover orientation or to potential temperature contamination from the rover. Thermal gradients in Figure 9c do not show a clear seasonal pattern either, beyond some time adjustments in LTST that follow the sunrise and sunset times along the Martian Year. Overall, with a few exceptions at particular locations, thermal gradients are negative during the daytime convective period and positive during the nighttime stable period (i.e., a thermal inversion occurs between the two main periods).

Interestingly, ATS temperature fluctuations at noon were most intense between L_S 200–315° and especially between L_S 270–315°. TIRS data also present maximum daytime fluctuations on MY36 between L_S 270–315°. This period is characterized by higher average dust opacity (Figure 4b), lower solar irradiance (Figure 4c) and lower activity of convective vortices (Hueso et al., 2023), which contrast with the presence of these unexpected intense temperature fluctuations. At the beginning of MY 37 during the early spring season, TIRS temperature fluctuations also intensified during both daytime and nighttime. Figures 9a and 9b and the rover path displayed in Figure 3 suggest that daytime fluctuations may have increased near the delta not by seasonal variations but due to the effects of the complex local topography on the observed meteorology. In contrast, nighttime temperature fluctuations at Jezero increased around L_S 180° and stayed relatively high during the dusty period (see Figures 9a and 9b), suggesting that seasonal effects might be present in nighttime temperature fluctuations. In contrast to these results, in an analysis of temperature data at Gale crater obtained by the Mars Science Laboratory, Mason et al. (2024) found a consistent seasonal pattern of daytime temperature fluctuations. Those authors found peaks in fluctuations during the period of maximum solar irradiance in results obtained over an extended period from MY31 to MY36 in which the Curiosity rover explored a diverse set of terrains over different elevations. The difference in the seasonal evolution of the intensity of thermal fluctuations between MSL data from Mason et al. (2024) and MEDA data shown here requires an explanation. Section 4 discusses ATS and TIRS temperature fluctuations and the stronger thermal gradients in terms of possible effects of the local meteorology near the delta's complex topography.

Right after the onset of dust storms at Jezero crater (on sols 315, 416 and 573), temperature fluctuations and thermal gradients seemed to weaken for a few sols, as observed in data from previous missions (e.g., Mason et al., 2024) and as predicted by Bertrand et al. (2016). The observed weakening of the convective instability during dust storms is well known and is associated with the absorption of shortwave radiation by atmospheric dust, which warms the atmosphere and reduces the surface-to-atmosphere temperature difference.

Occasionally, the thermal inversion seems absent from some nighttime observations. These generally occur in locations where the local terrain has anomalously large values of TI (Munguira et al., 2023; Rodríguez-Manfredi et al., 2023; Savijärvi et al., 2023). In contrast, the thermal inversion seems strongest around L_S 180° in Figure 9c, which might be supported by MCD predictions to a certain extent (Figure 9d).

Finally, the lowest temperature fluctuations are typically found during the CBL collapse, which translates into a pre-sunset dark band around 17 LTST in Figures 9a and 9b. Seasonal variations in the time of the CBL collapse are now discussed.

3.5. Time of CBL Collapse Over One Martian Year

The diurnal cycle of temperatures at Jezero is characterized by a convective regime at daytime and a stable regime at nighttime, with two transitions in between. These two transitions are asymmetric. The early morning transition occurs gradually as the surface heats at a rate different from the near surface atmosphere. The afternoon transition is characterized by a faster collapse of the CBL, during which thermal fluctuations completely disappear and the near surface thermal gradient vanishes (Munguira et al., 2023). MEDA data enable direct derivation of the time of the CBL collapse by means of finding the times of the sol with minimum temperature fluctuations and nearly null thermal gradients. We note that an evaluation of the Monin-Obukhov Length (MOL) from MEDA data could also be used to characterize the collapse of the CBL, since the MOL changes signify transitions between the unstable to stable periods (Martínez et al., 2009; Monin & Obukhov, 1954). However, estimating MOL requires knowledge of wind speeds that were not available after sol 315 and further assumptions such as horizontal homogeneity and flat terrain. In this section, we quantify the changes in the time of the CBL collapse at Jezero during MY 36, and examine whether these changes are linked to the seasonal evolution or to variations in the local conditions associated with different terrains.

We have looked at three different magnitudes to derive the time of the CBL collapse: (a) Temperature fluctuations measured with ATS at 1.45 m. (b) Temperature fluctuations at the first tens of meters measured with TIRS. (c) Temperature differences between the surface and the atmospheric level sampled with TIRS. In addition, we also examine temperature differences in MCD data between the surface and the atmosphere at 40 m as a control of the expected time of the CBL collapse that is independent of MEDA data and is not influenced by variations in the local conditions explored by the rover. For methods a and b, the time of the CBL collapse for each sol is retrieved as the time between 16 and 18 at which σ_T is minimum and falls below the instrument noise level (~ 0.1 K in ATS and ~ 0.35 K in TIRS). For method c and our external control from MCD data, the time of the CBL collapse for each sol is retrieved when thermal differences are closest to zero and also disregarding cases in which these minimum thermal differences are above 0.1 K to filter out artifacts. In addition, our results from methods a and b are examined by averaging values of σ_T at each LTST in subsets of 10 sols. This counteracts the effects of measurement gaps in the data and is the same technique used by Munguira et al. (2023). Moreover, we performed a visual inspection of the σ_T data to identify and disregard sols affected by measurement artifacts. An example of these artifacts is presented in Figure S1.

Figure 10a shows the times of the CBL collapse retrieved using these methods and our external control. Error bars are set to ± 5 min for method a, which is the time resolution after averaging all data in 5-min windows. We consider a longer error bar of ± 10 min in method b to account for the noisier records of TIRS. For method c, we interpolate the times of the CBL collapse retrieved from sols with adequate data, and then, we use a running average of 100 sols (solid gray line in Figure 10a) to smooth the sol-to-sol variability. Error bars for method c correspond to the standard deviation of the running average centered at each point and are more prominent at periods with less data.

The time of the CBL collapse retrieved from methods a, b and c follow similar seasonal trends over the whole MY 36, as shown in Figure 10a. Timings at the start of MY37 coincide with those at the beginning of the mission ($L_S 5^\circ$, MY 36), further supporting an annual cycle. Overall, the time of the CBL collapse seems to occur earlier than sunset by a fixed time of ~ 1 hr, except between sols 400 and 600 during which the CBL collapse drifted toward later times. Our control with MCD predicts the CBL collapse to occur earlier than sunset by ~ 0.5 hr without significant variations in the Martian year. The fixed time difference between the sunset and the CBL collapse indicates that the CBL collapse (and possibly CBL development) is mainly determined by the seasonal irradiance during most of the MY. However, the CBL collapse between sols 400 and 600 occurred relatively late (closer to sunset).

Since sols 400–600 ($\sim L_S 200\text{--}330^\circ$) encompass the dusty period of MY36 (Figure 4b), the CBL collapse may have been delayed due to the higher amount of dust in the atmosphere. Results from Large Eddy Simulations of the CBL performed by Bertrand et al. (2016) showed that the atmospheric dust load may modulate the strength of the convective instability (and consequently the CBL depth) and the time of the CBL collapse. Although a higher dust load usually decreases the surface-to-atmosphere gradient, and therefore, the convective instability,

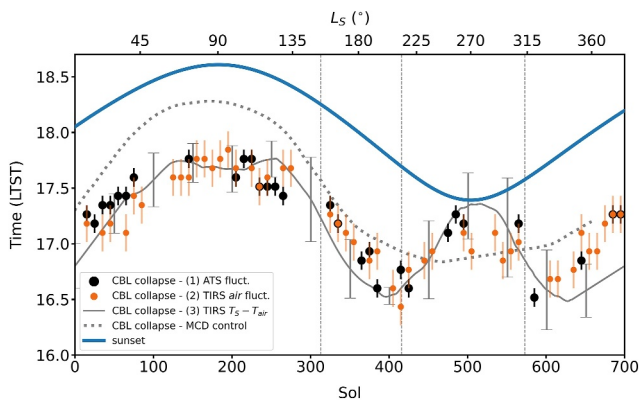


Figure 10. Time at which the convective boundary layer collapses at Jezero as a function of mission sol and L_S . The timings have been retrieved following three different methods and an external control from the analysis of Mars climate database data (see text and legend). Error bars illustrate the uncertainty of each measurement. The blue line indicates the time of the sunset as a function of season at Jezero. Vertical dotted lines indicate the onsets of dust storms at Jezero, as shown in Figure 4.

Section 3.4 shows intense ATS temperature fluctuations occurring at noon between sols 400 and 600 (Figure 9a). These fluctuations along with the thermal gradients in Figure 9c may support a strengthening of the convective instability during that period, which typically results in a later time for the CBL collapse (e.g., Bertrand et al., 2016). MEDA measurements in the next MYs will determine whether the delay in the CBL collapse is due to the increased dust load (repeated annually) or the local enhancement of convective activity during this specific period of MY 36 (e.g., Section 4).

4. Topographically Induced Variations in the Daytime Convective Instability

Besides albedo and TI, temperatures can be affected by local topography. For example, subtle and short-term changes in local temperatures associated with radiative effects from the different heating of nearby east/west facing slopes were described by Miller et al. (2018). In Section 3.4, we showed an increase in daytime convective instability as the rover approached the delta. This occurred during northern hemisphere winter, when mean daily air and surface temperatures are minimum near the surface (Figure 5) and when dust opacity in the atmosphere is the highest (Figure 4b). Surface albedo is also higher in the region traversed by Perseverance in this period, while variations in surface

TI are negligible compared with previous terrains (see Figure 2 in Martínez et al., 2024). Here we explore the possible impact of the topography on the increase in daytime vertical thermal gradients and temperature fluctuations near the delta.

To better quantify the increase in temperature oscillations, we show in Figure 11a ATS and TIRS air temperature fluctuations around noon (11:30–12:30 LTST). Maximum ATS temperature fluctuations occur between L_S 200 and 315°, while TIRS temperature fluctuations start to increase at L_S 270°, decay after the onset of the C storm and later recover their increasing trend. Note that ATS records local environmental temperatures near the surface, whereas TIRS is an infrared radiometer that is sensitive to average conditions of a layer of the atmosphere tens of meters high (Smith et al., 2023). Figures 11b and 11c display the vertical thermal gradient around noon and the rover elevation with respect to the landing site. This elevation is used to illustrate the rover's approach to the delta, since the ground at Jezero slopes upwards toward it. The figure shows how the vertical thermal gradient increased as the rover ascended and entered the delta. However, the elevation difference is too small to explain changes in the thermal gradient and the analysis of the data does not support a linear relation between both magnitudes.

Because the atmospheric opacity (Figure 4b), TI and albedo cover a wide range of values between sols 379 and 700 (Section 2.3), while the daytime thermal gradient is consistently higher during the whole period, we suggest that the observed increase in vertical instability is not related to variations in TI, albedo or dust load. For example, we note that thermal gradients and TIRS fluctuations near noon remained high at the beginning of MY 37 (sols 659–700; L_S 0–20°) when the atmospheric dust opacity had already decreased following its annual cycle. Instead, we suggest that the local meteorology changed near the delta due to the complex topography of the area. Winds predicted by models presented in Newman et al. (2021) show minimum wind speeds around L_S 270° with winds ascending over the crater walls and delta fan during the daytime. However, the still ongoing but unfinished retrievals of MEDA wind data during this period due to the deteriorated wind sensors do not allow us to explore changes in the wind regimes and how they could affect the temperature instabilities observed during this period.

5. Gravity Waves Effects on Near-Surface Temperature

The stable stratification of the nighttime Martian near surface atmosphere allows the propagation of gravity waves (GWs) down to the surface. GWs have been detected on Mars surface pressure data from MSL (Guzewich et al., 2021; Haberle et al., 2014), Insight (Banfield et al., 2020) and Perseverance data (Sánchez-Lavega, del Rio-Gaztelurrutia, et al., 2023), and have also been suggested in temperatures for a few sols on Gale (Miller et al., 2018). However, characterization of GW perturbations on near-surface temperatures has remained elusive for a long time for two reasons: (a) while pressure measurements account for the whole column of air above, GWs have to propagate all the way down to the surface to be observed on temperatures. (b) Near the surface, most

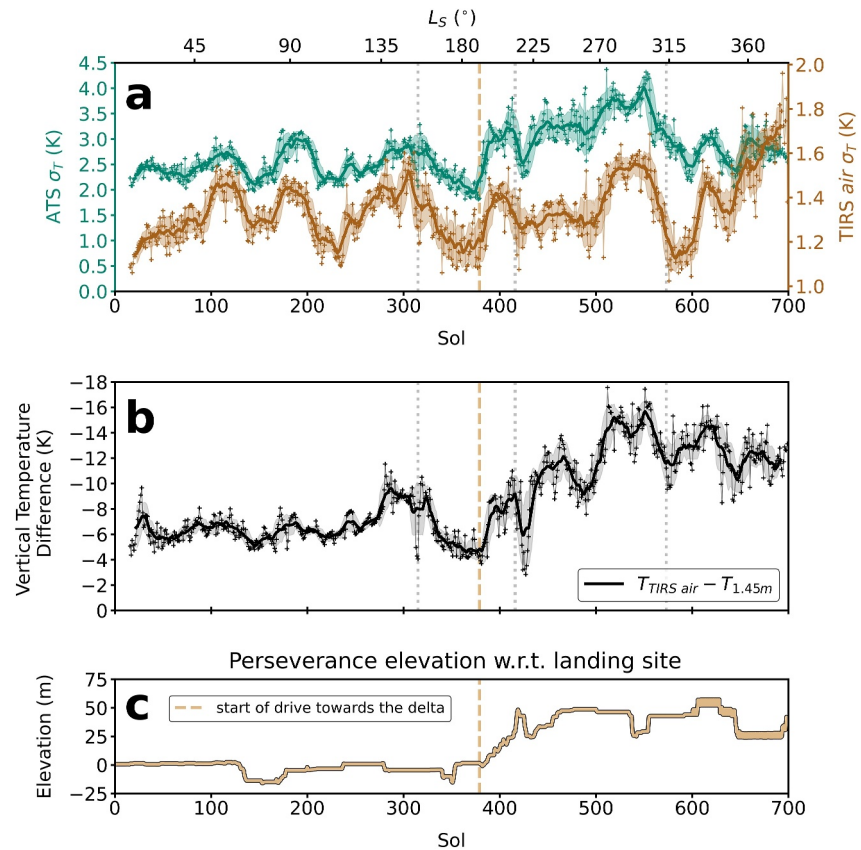


Figure 11. Change in the near-noon convective instability as a function of sol and L_S . (a) Air temperature fluctuations at $z = 1.45$ m (green) and thermal infrared sensors air level at around $z = 40$ m (brown) averaged between 11:30 and 12:30 local true solar time (LTST) as a function of sol and L_S . (b) Vertical thermal gradient (black, y-axis reversed) averaged between 11:30 and 12:30 LTST as a function of sol and L_S . The left y-axis is reversed to highlight the strongest instabilities (negative values of the vertical temperature difference). Running averages of 15 sols have been applied to all meteorological data (thick lines) to focus on the trends, with the shaded regions showing the standard deviations implied. (c) Perseverance elevation with respect to the landing site as a function of sol and L_S . The vertical dashed line in cream color marks the start of the rover's Rapid Traverse toward the delta. Vertical dotted lines indicate the onset of dust storms at Jezero.

gravity waves only contribute minor amplitudes on temperature variations and they can be easily masked by fast thermal variations caused by turbulence and by low-frequency artifacts in the data produced by the rover's boundary layer. Spectral methods have been applied to Mars surface pressure data obtained by Insight in a continuous sequence (i.e., without sampling gaps) to discern among turbulence and GWs (Temel et al., 2022). While the applicability of these methods to MEDA temperatures with gaps in the data is not straightforward, adapted spectral methods for sub-sets of MEDA temperatures should be tested in the future prior to analyzing the entire MEDA data set in search for additional potential GW events. In this section, we present an event of nighttime pressure and temperature oscillations observed by MEDA with frequencies and amplitudes that are consistent with a GW.

Figure 12a shows pressure oscillations detected by MEDA's pressure sensor in the evening of sol 523 ($L_S 282^\circ$). The maximum amplitudes of the pressure oscillations shown in Figure 12a are ~ 0.4 Pa, and their dominant period is ~ 10 min, similar to the 12–24 min periods detected in GWs in previous sols at Jezero (Sánchez-Lavega, del Rio-Gaztelurrutia, et al., 2023). Guzewich et al. (2021) reported gravity waves from pressure data with similar (and larger) periods at Curiosity's location with strongest activity in the late evening and early morning and between $L_S 180$ – 360° , that is, within the seasonal period of the event in Figure 12. The shorter period in the event on sol 523 requires stronger static stability and more stable conditions than in the cases reported in those studies.

Figures 12b and 12c show simultaneous oscillations in air temperature at 1.45 m and at tens of meters measured by ATS1 and TIRS, respectively. Here, we only show one of the three ATS sensors at 1.45 m to avoid masking the

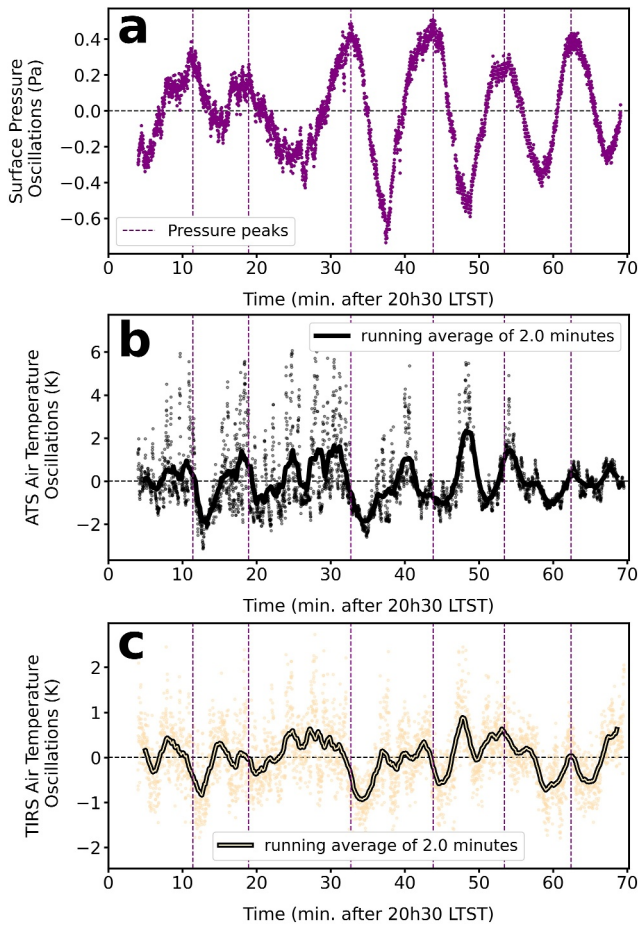


Figure 12. Gravity wave perturbations observed on near-surface pressure and temperatures after 20:30 LTST on sol 523. Panels (a–c) show the oscillations recorded by Mars environmental dynamics analyzer (MEDA) in pressure, air temperature sensors (ATS) and thermal infrared sensors air temperatures, respectively. In the three panels, MEDA measurements at 1 Hz (represented by dots) are shown after detrending the diurnal evolution through 3rd order polynomials. ATS and TIRS' high-frequency data are smoothed with a running average in 2-min windows (solid lines). Vertical purple lines indicate peaks in the amplitude of pressure oscillations.

temperature oscillations by superimposing data from other sensors. However, ATS2, ATS3 and ATS5—the latter located at 0.84 m—all measure equivalent oscillations. Running averages of 2 min are used here to remove higher frequency oscillations in temperature caused by local turbulence. The fact that all ATS sensors (except ATS4 that is often over warmed due to its difficulty to efficiently couple with the atmosphere because of its location behind the rover's arm, see Munguira et al., 2023) and the TIRS air channel measure the same temperature oscillations indicates that the oscillations are actually related to the atmosphere, rather than caused by thermal contamination from the rover. These temperature oscillations show wave-like behavior that resembles the GWs on pressure. In particular, many local minimums in temperatures occur 2 min after maximum peaks in pressure (vertical purple lines in Figure 12), suggesting an average phase shift between pressure and temperature oscillations. Note that pressure sensors detect GWs sooner than temperature sensors since they are sensitive to the atmospheric column above. The average phase shift of 2 min between pressure and temperature oscillations seems to change over the time series. This apparent change in the time shift may be due to temperature oscillations being influenced not only by GWs above but also by the atmospheric flow close to the surface (Nappo, 2013).

Comparing similar features in Figures 12b and 12c, we estimate that temperature oscillations are observed ~ 20 s sooner in TIRS than in ATS, suggesting a downward propagation of the GW. If we consider that TIRS air measurements correspond to a height of 40 m (the nominal atmospheric level of highest sensitivity for TIRS IR2 channel) and know that ATS1 is located at 1.45 m, we can infer a lower limit to the vertical velocity of the wave of $w \sim 2$ m/s.

At the time of the event, mean temperatures were 201, 206 and 204 K at the surface, 1.45 and ~ 40 m, respectively. These measurements suggest that the GW event occurred under conditions of moderate stability, with a temperature difference between the air and the surface of ~ 5 K for ATS and ~ 3 K for TIRS.

For an air parcel oscillating around its equilibrium level the Brunt-Väisälä frequency N is given by (e.g., Sánchez-Lavega, 2010):

$$N = \sqrt{g \frac{\Gamma_d - \Gamma}{T_a}}$$

On Mars, the acceleration of gravity is $g = 3.71$ m/s² and the dry adiabatic lapse rate is $\Gamma_d = -\frac{dT}{dz} = \frac{g}{c_p} \approx 4.5 \cdot 10^{-3}$ K/m. For the air temperature (T_a), we take the average of the two atmospheric levels (ATS at 1.45 m and TIRS air level), that is, $T_a = 205$ K. Since the nighttime thermal gradient is weak, we examine two extreme values for Γ : An isothermal atmosphere with $\Gamma = 0$, and a vertical lapse rate $\Gamma = -\frac{dT}{dz} \approx -75 \cdot 10^{-3}$ K/m from the TIRS surface and air temperatures. These values lead to a range of Brunt-Väisälä frequencies of $N = 0.009$ – 0.038 s⁻¹. From these values, the range of minimum periods associated with a GW is 11.6–2.76 min. Assuming a purely vertical propagation of the GW, the observed period of 10 min is closer to a purely isothermal atmosphere, requiring a small thermal gradient of $\Gamma = -\frac{dT}{dz} = -1.6 \cdot 10^{-3}$ K/m, which might be representative of the lapse rate of the atmosphere very close to the surface where the GW was observed.

The event here reported and detected on sol 523 was unique. While Sánchez-Lavega, del Rio-Gaztelurrutia, et al. (2023) found many other cases of GWs in their analysis of MEDA surface pressure, this was a particularly intense GW in pressure, with the shortest period and the only clear event in 700 sols found simultaneously in near surface temperatures. On sol 523, the rover was located close to the delta's topographic slopes (green star in

Figure 3) that lie to the NW, and the nighttime radiative cooling should produce topographic winds descending from the crater rim (Newman et al., 2021). Thus, it is reasonable to assume that the wave fronts might have come from the NW too, and that the delta's complex topography was related to the source of the GWs observed on sol 523.

Lastly, we would expect that gravity waves would contribute higher amplitudes to the temperatures at higher atmospheric levels. While MEDA observes more intense oscillations in ATS (~ 2 K for low-frequency oscillations) as compared to TIRS air temperatures (~ 1 K), this may be associated with TIRS' oscillations being smoothed due to the sensitivity of TIRS to multiple height levels as the wave was propagating downwards. In addition, the rover stayed at the same location for sols 515–535 finding regular events of weaker gravity waves on the pressure data at the same LTST, but without clear signatures in temperature. The time delay between TIRS and ATS signals suggesting a downward propagation, the local topography, and the detection at the time of near isothermal lapse rate are all consistent with internal gravity waves generated by shear at the interface between the free atmosphere and the stably stratified layer near the ground (e.g., Sun et al., 2015).

6. Conclusions

We have presented the near-surface temperatures on Jezero during a full Martian Year. Seasonal effects are present in the diurnal cycle, including the thermal tides, and in oscillations of mean daily temperatures associated with atmospheric waves. Furthermore, the rover's journey toward the delta and its complex topography introduced additional complexity and variability in local temperatures. In the following, we summarize and discuss the main takeaways of this work.

Seasonal variations in daily mean temperatures at the surface and atmosphere are mainly determined by the daily irradiance at the surface. A reference model like MCD accurately predicts these mean seasonal variations. In addition, daily maximum temperatures at Jezero, which are more variable than minimum temperatures during the MY, peak at $L_S 180^\circ$ coinciding with the maximum irradiance. At this time, maximum temperatures are ~ 10 K warmer in MEDA than in MCD and we suggest that low-altitude dust could explain the difference. However, other periods of the MY also result in higher temperatures in MEDA data than in MCD, which could be associated with incomplete model parameterizations of the turbulence near the surface on Mars.

MEDA's cadence allowed us to investigate the thermal tides in the temperature signal. The amplitude of the diurnal mode of the thermal tides responds to the seasonal irradiance cycle and dust storms. Additional oscillations of 3–5 K with respect to the mean values of the diurnal tide are observed with time scales of tens of sols without a clear influence from variations in irradiance. In turn, the semidiurnal and terdiurnal modes present little response to the seasonal irradiance cycle. Both have similar amplitudes during the aphelion season and opposing trends during the dusty season, when the semidiurnal mode is most prominent and the terdiurnal mode is negligible. Dust storms produce smaller effects in temperatures than in pressure, confirming a moderate response of near-surface temperatures to the global dynamics.

Oscillations in daily mean temperatures likely associated with traveling waves with periods of a few sols have also been detected. Before $L_S 120^\circ$ we observed a quiet period with sol-to-sol variations in mean temperatures always below 0.5 K. After $L_S 180^\circ$ sol-to-sol variations in temperature intensified, especially after $L_S 300^\circ$. In this period, we detected wave amplitudes in the mean daily air temperature of 1.5 K, with mean periods of 3–7 sols. Two times of small oscillations between $L_S 180$ – 360° are the solsticial pause ($L_S 270^\circ$) and the aftermath of the C storms, both of which had been previously reported at other locations. The GCM used in MCD produces similar results with a quiet and an active period with similar seasonal behavior and wave amplitudes. We suggest that the thermal oscillations in mean temperatures found here are caused by the enhanced baroclinic activity in northern mid-latitudes that occurs during the perihelion season (Barnes, 1980).

Daytime fast fluctuations of temperature and vertical thermal gradients, roughly indicative of the daytime convective activity, do not show clear seasonal trends and instead they peak during northern hemisphere winter (i.e., during minimum solar irradiance) when Perseverance was located at the delta front. We interpret the intensified thermal gradients and increased temperature fluctuations found during that period as a consequence of local meteorology with an interplay between winds and the intricate topography of the delta.

We have found that the time of the CBL collapse occurs 1 hr before sunset during most seasons at Jezero. A delay in the time of the CBL collapse was observed between sols 400 and 600 ($L_S 200$ – 330°) coinciding with the dustier period of the MY. It remains to be assessed whether the delay is repeated annually during the dusty period or if

this was a consequence of the rover's location at the delta front and the anomalous intense convective activity detected during that period.

Lastly, simultaneous temperature and pressure oscillations consistent with gravity waves were detected near the delta region at 20:30 LTST on sol 523. We estimate an average period of 10 min for the GWs with amplitudes of 0.4 Pa, 2 and 1 K for oscillations in pressure, ATS temperatures and TIRS temperatures, respectively.

Studying near-surface temperatures is essential to understand PBL processes on Mars, validate atmospheric models and design future missions to the surface of Mars. The present study suggests an impact of the delta's topography on the local meteorology. However, the underlying physical mechanisms are unclear. Future analyses extending over later sols beyond sol 700 would have to consider the characteristics of the terrain in a more complex location than in Munguira et al. (2023) (covering the crater floor) or this work (also covering the approach to the crater rim). High-resolution atmospheric modeling will be essential to investigate local meteorological variations as those found in Jezero's delta front.

Data Availability Statement

The MEDA data used in this study are available via the NASA Planetary Data System (PDS) (Rodríguez-Manfredi et al., 2021b). Ancillary data used in Figure 11c are also available at the PDS. The software to derive MEDA ATS temperatures at 1.45 m from raw MEDA ATS data is available at Zenodo (Hueso et al., 2022). In the same repository, we have included a new version (Version 2) with processed data needed to generate and reproduce the figures in this study. Albedo and thermal inertia values are obtained from MEDA data following the procedure in Martínez et al. (2023). These values were extended up to sol 700 in Figure 2 in Martínez et al. (2024). Atmospheric opacities at Jezero are calculated from publicly available data from the ZCAM instrument via the PDS (Bell & Maki, 2021). The Mars Climate Database (MCD) is accessible at https://www-mars.lmd.jussieu.fr/mcd_python/ (Colaïtis et al., 2013; Forget et al., 1999; Millour et al., 2017). Some figures have been designed using color palettes from Crameri et al. (2020).

References

- Arya, P. S. (2001). *Introduction to micrometeorology*. Academic Press.
- Banfield, D., Spiga, A., Newman, C. E., Forget, F., Lemmon, M. T., Lorenz, R. D., et al. (2020). The atmosphere of Mars as observed by InSight. *Nature Geoscience*, 13(3), 190–198. <https://doi.org/10.1038/s41561-020-0534-0>
- Barnes, J. R. (1980). Time spectral analysis of midlatitude disturbances in the Martian atmosphere. *Journal of the Atmospheric Sciences*, 37(9), 2002–2015. [https://doi.org/10.1175/1520-0469\(1980\)037<2002:TSAOMD>2.0.CO;2](https://doi.org/10.1175/1520-0469(1980)037<2002:TSAOMD>2.0.CO;2)
- Barnes, J. R. (1981). Midlatitude disturbances in the Martian atmosphere: A second Mars year. *Journal of the Atmospheric Sciences*, 38(2), 225–234. [https://doi.org/10.1175/1520-0469\(1981\)038<0225:MDITMA>2.0.CO;2](https://doi.org/10.1175/1520-0469(1981)038<0225:MDITMA>2.0.CO;2)
- Barnes, J. R. (1984). Linear baroclinic instability in the Martian atmosphere. *Journal of the Atmospheric Sciences*, 41(9), 1536–1550. [https://doi.org/10.1175/1520-0469\(1984\)041<1536:LBIITM>2.0.CO;2](https://doi.org/10.1175/1520-0469(1984)041<1536:LBIITM>2.0.CO;2)
- Battalio, J. M., Martínez, G., Newman, C., de la Torre Juárez, M., Sánchez-Lavega, A., & Víudez-Moreiras, D. (2022). Planetary waves traveling between Mars science laboratory and Mars 2020. *Geophysical Research Letters*, 49(21), e2022GL100866. <https://doi.org/10.1029/2022GL100866>
- Bell, J. F., & Maki, J. N. (2021). Mars 2020 mast camera zoom bundle, from Arizona state University Mastcam-z instrument team, calibrated products [Dataset]. *NASA Planetary Data System*. <https://doi.org/10.17189/Q3TS-C749>
- Bell, J. F., Maki, J. N., Alwmark, S., Ehlmann, B. L., Fagents, S. A., Grotzinger, J. P., et al. (2022). Geological, multispectral, and meteorological imaging results from the Mars 2020 perseverance rover in Jezero crater. *Science Advances*, 8(47), eabo4856. <https://doi.org/10.1126/sciadv.abo4856>
- Bertrand, T., Spiga, A., Rafkin, S., Colaïtis, A., Forget, F., & Millour, E. (2016). An intercomparison of Large-Eddy Simulations of the Martian daytime convective boundary layer. *Geoscientific Model Development Discussions*. <https://doi.org/10.5194/gmd-2016-241>
- Chatain, A., Spiga, A., Banfield, D., Forget, F., & Murdoch, N. (2021). Seasonal variability of the daytime and nighttime atmospheric turbulence experienced by InSight on Mars. *Geophysical Research Letters*, 48(22), e2021GL095453. <https://doi.org/10.1029/2021GL095453>
- Cheng, Y., Parlange, M. B., & Brutsaert, W. (2005). Pathology of Monin-Obukhov similarity in the stable boundary layer. *Journal of Geophysical Research*, 110(D6), D06101. <https://doi.org/10.1029/2004JD004923>
- Chide, B., Bertrand, T., Lorenz, R. D., Munguira, A., Hueso, R., Sánchez-Lavega, A., et al. (2022). Acoustics reveals short-term air temperature fluctuations near Mars' surface. *Geophysical Research Letters*, 49(21), e2022GL100333. <https://doi.org/10.1029/2022GL100333>
- Colaïtis, A., Spiga, A., Hourdin, F., Rio, C., Forget, F., & Millour, E. (2013). A thermal plume model for the Martian convective boundary layer. *Journal of Geophysical Research: Planets*, 118(7), 1468–1487. <https://doi.org/10.1002/jgre.20104>
- Crameri, F., Shephard, G. E., & Heron, P. J. (2020). The misuse of colour in science communication. *Nature Communications*, 11(1), 5444. <https://doi.org/10.1038/s41467-020-19160-7>
- de la Torre Juárez, M., Chavez, A., Tampari, L. K., Munguira, A., Martínez, G., Hueso, R., et al. (2023). Diurnal cycle of rapid air temperature fluctuations at Jezero Crater: Probability distributions, exponential tails, scaling, and intermittency. *Journal of Geophysical Research: Planets*, 128(7), e2022JE007458. <https://doi.org/10.1029/2022JE007458>

Acknowledgments

The authors are very grateful to the entire Mars 2020 science operations team. We would also like to thank Orkun Temel and an anonymous reviewer for their comments, which helped us to improve the quality of the manuscript. AM is supported by the grant PRE2020-092562 funded by MCIN/AEI/10.13039/501100011033 and by "ESF Investing in your future." RH, ASL and TdRG are supported by Grant PID2019-109467GB-I00 funded by MCIN/AEI/10.13039/501100011033/. AM, RH, ASL and TdRG are supported by Grupos Gobierno Vasco IT1742-22. Part of this work was carried out at the Jet Propulsion Laboratory/California Institute of Technology under a NASA-STMD grant, and under a contract with the National Aeronautics and Space Administration (80NM0018D0004). AVR is funded by the Spanish Ministry of Science and Innovation (MCIN)/State Agency of Research (AEI) project PID2021-126719OB-C41, funded by MCIN/AEI/10.13039/501100011033/ FEDER, UE.

- de la Torre Juárez, M., Piqueux, S., Kass, D. M., Newman, C. E., & Guzewich, S. D. (2024). Pressure deficit in Gale crater and a larger northern polar cap after the MY34 global dust storm. *Journal of Geophysical Research: Planets*, 129(1), e2023JE007810. <https://doi.org/10.1029/2023JE007810>
- Forget, F., Hourdin, F., Fournier, R., Hourdin, C., Talagrand, O., Collins, M., et al. (1999). Improved general circulation models of the Martian atmosphere from the surface to above 80 km. *Journal of Geophysical Research*, 104(E10), 24155–24176. <https://doi.org/10.1029/1999JE001025>
- Gómez-Elvira, J., Armiens, C., Carrasco, I., Genzer, M., Gómez, F., Haberle, R., et al. (2014). Curiosity's rover environmental monitoring station: Overview of the first 100 sols. *Journal of Geophysical Research: Planets*, 119(7), 1680–1688. <https://doi.org/10.1002/2013JE004576>
- Guzewich, S. D., de la Torre Juárez, M., Newman, C. E., Mason, E., Smith, M. D., Miller, N., et al. (2021). Gravity wave observations by the Mars Science Laboratory REMS pressure sensor and comparison with mesoscale atmospheric modeling with MarsWRF. *Journal of Geophysical Research: Planets*, 126(8), e2021JE006907. <https://doi.org/10.1029/2021JE006907>
- Guzewich, S. D., Newman, C. E., de la Torre Juárez, M., Wilson, R. J., Lemmon, M., Smith, M. D., et al. (2016). Atmospheric tides in Gale crater, Mars In. *Icarus* (Vol. 268, pp. 37–49). Elsevier BV. <https://doi.org/10.1016/j.icarus.2015.12.028>
- Haberle, R. M., de la Torre Juárez, M., Kahre, M. A., Kass, D. M., Barnes, J. R., Hollingsworth, J. L., et al. (2018). Detection of northern hemisphere transient eddies at Gale crater Mars. *Icarus*, 307, 150–160. <https://doi.org/10.1016/j.icarus.2018.02.013>
- Haberle, R. M., Gómez-Elvira, J., de la Torre Juárez, M., Harri, A., Hollingsworth, J. L., Kahanpää, H., et al. (2014). Preliminary interpretation of the REMS pressure data from the first 100 sols of the MSL mission. *Journal of Geophysical Research: Planets*, 119(3), 440–453. <https://doi.org/10.1002/2013JE004488>
- Hess, S. L., Henry, R. M., Leovy, C. B., Ryan, J. A., & Tillman, J. E. (1977). Meteorological results from the surface of Mars: Viking 1 and 2. *Journal of Geophysical Research*, 82(B28), 4559–4574. <https://doi.org/10.1029/J082i028p04559>
- Hess, S. L., Ryan, J. A., Tillman, J. E., Henry, R. M., & Leovy, C. B. (1980). The annual cycle of pressure on Mars measured by Viking Landers 1 and 2. *Geophysical Research Letters*, 7(3), 197–200. <https://doi.org/10.1029/GL007i003p0197>
- Hueso, R., Munguira, A., Sánchez-Lavega, A., De la Torre-Juárez, M., Rodríguez-Manfredi, J., & Lepinette, A. (2022). Derived environmental temperatures at Jezero crater from air temperature sensors' measurements on the perseverance rover [Dataset]. *Zenodo*. <https://doi.org/10.5281/zenodo.7461834>
- Hueso, R., Newman, C., del Río-Gaztelurrutia, T., Munguira, A., Sánchez-Lavega, A., Toledo, D., et al. (2023). Vortices and dust devils at Jezero crater after one year of measurements with MEDA on Mars 2020. *EGU General Assembly 2023*. <https://doi.org/10.5194/egusphere-egu23-6062>
- Jiang, C., Jiang, Y., Li, H., & Du, S. (2023). Initial results of the meteorological data from the first 325 sols of the Tianwen-1 mission. *Scientific Reports*, 13(1), 3325. <https://doi.org/10.1038/s41598-023-30513-2>
- Kahre, M. A., Murphy, J. R., Newman, C. E., Wilson, R. J., Cantor, B. A., Lemmon, M. T., et al. (2017). The Mars dust cycle. In R. M. Haberle, R. T. Clancy, F. Forget, M. D. Smith, & R. W. Zurek (Eds.), *The atmosphere and climate of Mars (Cambridge planetary science* (pp. 295–337). Cambridge University Press. <https://doi.org/10.1017/9781139060172.010>
- Kass, D. M., Kleinböhl, A., McCreese, D. J., Schofield, J. T., & Smith, M. D. (2016). Interannual similarity in the Martian atmosphere during the dust storm season. *Geophysical Research Letters*, 43(12), 6111–6118. <https://doi.org/10.1002/2016GL068978>
- Kempenaar, J., Novak, K., Redmond, M., Farias, E., Singh, K., & Wagner, M. (2018). Detailed surface thermal design of the Mars 2020 rover. In *48th international conference on environmental systems*. Retrieved from <http://hdl.handle.net/2346/74064>
- Lemmon, M. T., Smith, M. D., Viudez-Moreiras, D., de la Torre Juárez, M., Vicente-Retortillo, A., Munguira, A., et al. (2022). Dust, sand, and winds within an active Martian storm in Jezero crater. *Geophysical Research Letters*, 49(17), e2022GL100126. <https://doi.org/10.1029/2022GL100126>
- Leovy, C. B. (1977). The atmosphere of Mars. *Scientific American*, 237(1), 34–43. <https://doi.org/10.1038/scientificamerican0777-34>
- Leovy, C. B., & Zurek, R. W. (1979). Thermal tides and Martian dust storms: Direct evidence for coupling. *Journal of Geophysical Research*, 84(B6), 2956–2968. <https://doi.org/10.1029/JB084iB06p02956>
- Lewis, S. R., Collins, M., Read, P. L., Forget, F., Hourdin, F., Fournier, R., et al. (1999). A climate database for Mars. *Journal of Geophysical Research*, 104(E10), 24177–24194. <https://doi.org/10.1029/1999je001024>
- Lewis, S. R., Mulholland, D. P., Read, P. L., Montabone, L., Wilson, R. J., & Smith, M. D. (2016). The solsticial pause on Mars: 1. A planetary wave reanalysis. *Icarus*, 264, 456–464. <https://doi.org/10.1016/j.icarus.2015.08.039>
- Martínez, G., Valero, F., & Vázquez, L. (2009). Characterization of the Martian surface layer. *Journal of the Atmospheric Sciences*, 66(1), 187–198. <https://doi.org/10.1175/2008JAS2765.1>
- Martínez, G. M., Newman, C. E., De Vicente-Retortillo, A., Fischer, E., Renno, N., Richardson, M., et al. (2017). The modern near-surface Martian climate: A review of in situ meteorological data from Viking to curiosity. *Space Science Reviews*, 212(1), 295–338. <https://doi.org/10.1007/s11214-017-0360-x>
- Martínez, G. M., Sebastián, E., Vicente-Retortillo, A., Smith, M. D., Johnson, J. R., Fischer, E., et al. (2023). Surface energy budget, albedo and thermal inertia at Jezero Crater, Mars, as observed from the Mars 2020 MEDA instrument. *Journal of Geophysical Research: Planets*, 128(2), e2022JE007537. <https://doi.org/10.1029/2022JE007537>
- Martínez, G. M., Vicente-Retortillo, A., Sebastián, E., Fischer, E., Smith, M., Savijärvi, H., et al. (2024). Albedo and thermal inertia for the first 777 sols of the Mars 2020 mission. In *55th lunar and planetary science conference*. Retrieved from <https://www.hou.usra.edu/meetings/lpsc2024/pdf/1975.pdf>
- Martín-Rubio, C., Vicente-Retortillo, A., Gómez, F., & Rodríguez-Manfredi, J. A. (2024). Interannual variability of regional dust storms between Mars years 24 and 36. *Icarus*, 412, 115982. <https://doi.org/10.1016/j.icarus.2024.115982>
- Mason, E. L., & Smith, M. D. (2021). Temperature fluctuations and boundary layer turbulence as seen by Mars exploration rovers miniature thermal emission spectrometer. *Icarus*, 360, 114350. <https://doi.org/10.1016/j.icarus.2021.114350>
- Mason, E. L., Smith, M. D., Richardson, M. I., & Guzewich, S. D. (2024). Comparing atmospheric temperature fluctuations across landed missions. *Journal of Geophysical Research: Planets*, 129(1), e2023JE007750. <https://doi.org/10.1029/2023JE007750>
- Miller, N. M., de la Torre Juárez, M., & Tamppari, L. (2018). The effect of Bagnold dunes slopes on the short timescale air temperature fluctuations at Gale Crater on Mars. *Geophysical Research Letters*, 45(21), 11588–11594. <https://doi.org/10.1029/2018GL080542>
- Millour, E., Forget, F., & Lewis, S. (2017). Mars climate database v. 5.3. User manual. *ESTEC Contract*. Retrieved from http://www-mars.lmd.jussieu.fr/mars/info_web/user_manual_5.3.pdf
- Millour, E., Forget, F., Spiga, A., Pierron, T., Bierjon, A., Montabone, L., et al. (2022). The Mars climate database (version 6.1). In *Europlanet science congress 2022* (Vol. 16). <https://doi.org/10.5194/epsc2022-786>
- Monin, A., & Obukhov, A. (1954). Osnovnye zakonomernosti turbulentnogo peremeshivaniya v prizemnom sloe atmosfery (basic laws of turbulent mixing in the atmosphere near the ground). *Trudy Geofiz. Inst. AN SSSR*, 24, 163.

- Montabone, L., Forget, F., Millour, E., Wilson, R. J., Lewis, S. R., Cantor, B., et al. (2015). Eight-year climatology of dust optical depth on Mars. In *Icarus* (Vol. 251, pp. 65–95). Elsevier BV. <https://doi.org/10.1016/j.icarus.2014.12.034>
- Munguira, A., Hueso, R., Sánchez-Lavega, A., de la Torre Juárez, M., Martínez, G. M., Newman, C. E., et al. (2023). Near surface atmospheric temperatures at Jezero from Mars 2020 MEDA measurements. *Journal of Geophysical Research: Planets*, 128(3), e2022JE007559. <https://doi.org/10.1029/2022JE007559>
- Nappo, C. J. (2013). *An introduction to atmospheric gravity waves*. Academic Press.
- Newman, C. E., de la Torre Juárez, M., Pla-García, J., Wilson, R. J., Lewis, S. R., Neary, L., et al. (2021). Multi-model meteorological and Aeolian predictions for Mars 2020 and the Jezero crater region. *Space Science Reviews*, 217(1), 20. <https://doi.org/10.1007/s11214-020-00788-2>
- Ordoñez-Etxeberria, I., Hueso, R., Sánchez-Lavega, A., Millour, E., & Forget, F. (2019). Meteorological pressure at Gale crater from a comparison of REMS/MSL data and MCD modelling: Effect of dust storms. *Icarus*, 317, 591–609. <https://doi.org/10.1016/j.icarus.2018.09.003>
- Patel, P., Tamppari, L., de la Torre Juárez, M., Lemmon, M., Coates, A., Wolff, M., et al. (2023). Geometric properties of water-ice clouds as observed from Jezero Crater in the first 600 sols with the NavCam instrument onboard Mars2020 rover, perseverance. *Planetary Science Journal*, 4(12), 226. <https://doi.org/10.3847/PSJ/acfc35>
- Pérez-Grande, I., Peinado, L., Chamorro, A., Torralbo, I., Alonso, G., Rodríguez Manfredi, J. A., et al. (2017). Thermal design of the Air Temperature Sensor (ATS) and the Thermal InfraRed Sensor (TIRS) of the Mars Environmental Dynamics Analyzer (MEDA) for Mars 2020. In *47th international conference on environmental systems*.
- Pla-García, J., Munguira, A., Rafkin, S., Newman, C., Bertrand, T., Martínez, G., et al. (2023). Nocturnal turbulence at Jezero crater as determined from MEDA measurements and modeling. *Journal of Geophysical Research: Planets*, 128(8), e2022JE007607. <https://doi.org/10.1029/2022JE007607>
- Read, P. L., Galperin, B., Larsen, S. E., Lewis, S. R., Määttänen, A., Petrosyan, A., et al. (2017). The Martian planetary boundary layer. In R. M. Haberle, R. T. Clancy, F. Forget, M. D. Smith, & R. W. Zurek (Eds.), *The atmosphere and climate of Mars (Cambridge planetary science)* (pp. 172–202). Cambridge University Press. <https://doi.org/10.1017/9781139060172.007>
- Read, P. L., Lewis, S. R., & Mulholland, D. P. (2015). The physics of Martian weather and climate: A review. *Reports on Progress in Physics*, 78(12), 125901. <https://doi.org/10.1088/0034-4885/78/12/125901>
- Rodríguez-Manfredi, J. A., de la Torre Juárez, M., Alonso, A., Apéstigue, V., Arruego, I., Atienza, T., et al. (2021a). The Mars environmental dynamics analyzer, Meda. A suite of environmental sensors for the Mars 2020 mission. *Space Science Reviews*, 217(3), 1–86. <https://doi.org/10.1007/s11214-021-00816-9>
- Rodríguez-Manfredi, J. A., de la Torre Juárez, M., Sánchez-Lavega, A., Hueso, R., Martínez, G., Lemmon, M. T., et al. (2023). The diverse meteorology of Jezero crater over the first 250 sols of Perseverance on Mars. *Nature Geoscience*, 16(1), 19–28. <https://doi.org/10.1038/s41561-022-01084-0>
- Rodríguez-Manfredi, J. A., de la Torre Juárez, M., Alonso, A., Apéstigue, V., Arruego, I., Atienza, T., et al. (2021b). The Mars environmental dynamics analyzer, MEDA [Dataset]. *NASA Planetary Data System*. https://atmos.nmsu.edu/PDS/data/PDS4/Mars2020/mars2020_meda/
- Ryan, J. A., & Henry, R. M. (1979). Mars atmospheric phenomena during major dust storms, as measured at the surface. *Journal of Geophysical Research*, 84(B6), 2821–2829. <https://doi.org/10.1029/JB084iB06p02821>
- Sánchez-Lavega, A. (2010). *An introduction to planetary atmospheres*. CRC Press, Taylor & Francis.
- Sánchez-Lavega, A., del Río-Gaztelurrutia, T., Hueso, R., de la Torre Juárez, M., Martínez, G. M., Harri, A.-M., et al. (2023). Mars 2020 Perseverance rover studies of the Martian atmosphere over Jezero from pressure measurements. *Journal of Geophysical Research: Planets*, 128(1), e2022JE007480. <https://doi.org/10.1029/2022JE007480>
- Sánchez-Lavega, A., Larsen, E., Hernández-Bernal, J., del Río-Gaztelurrutia, T., Ordóñez-Etxeberria, I., & Cardesin Moineo, A. (2023). Planetary and synoptic-scale atmospheric disturbances from images of Mars during Martian Year 36. *EGU General Assembly*. <https://doi.org/10.5194/egusphere-egu23-8619>
- Savijärvi, H. I., Martínez, G. M., & Harri, A.-M. (2023). Surface energy fluxes and temperatures at Jezero crater, Mars. *Journal of Geophysical Research: Planets*, 128(2), e2022JE007438. <https://doi.org/10.1029/2022JE007438>
- Sebastián, E., Martínez, G. M., Ramos, M., Haenschke, F., Ferrándiz, R., Fernández, M., & Manfredi, J. A. R. (2020). Radiometric and angular calibration tests for the MEDA-TIRS radiometer onboard NASA's Mars 2020 mission. *Measurement*, 164, 107968. <https://doi.org/10.1016/j.measurement.2020.107968>
- Sebastián, E., Martínez, G. M., Ramos, M., Pérez-Grande, I., Sobrado, J., & Manfredi, J. A. R. (2021). Thermal calibration of the MEDA-TIRS radiometer onboard NASA's perseverance rover. *Acta Astronautica*, 182, 144–159. <https://doi.org/10.1016/j.actaastro.2021.02.006>
- Smith, M. D., Martínez, G. M., Sebastián, E., Lemmon, M. T., Wolff, M. J., Apéstigue, V., et al. (2023). Diurnal and seasonal variations of aerosol optical depth observed by MEDA/TIRS at Jezero Crater, Mars. *Journal of Geophysical Research: Planets*, 128(1), e2022JE007560. <https://doi.org/10.1029/2022JE007560>
- Smith, M. D., Wolff, M. J., Lemmon, M. T., Spanovich, N., Banfield, D., Budney, C. J., et al. (2004). First atmospheric science results from the Mars exploration Rovers Mini-Tes. *Science*, 306(5702), 1750–1753. <https://doi.org/10.1126/science.1104257>
- Smith, M. D., Wolff, M. J., Spanovich, N., Ghosh, A., Banfield, D., Christensen, P. R., et al. (2006). One Martian year of atmospheric observations using MER Mini-TES. *Journal of Geophysical Research*, 111(E12), E12S13. <https://doi.org/10.1029/2006JE002770>
- Stull, R. B. (1988). *An introduction to boundary layer meteorology*. Springer. <https://doi.org/10.1007/978-94-009-3027-8>
- Sun, J., Mahrt, L., Nappo, C., & Lenschow, D. H. (2015). Wind and temperature oscillations generated by wave-turbulence interactions in the stably stratified boundary layer. *Journal of the Atmospheric Sciences*, 72(4), 1484–1503. <https://doi.org/10.1175/JAS-D-14-01>
- Sun, V. Z., Hand, K. P., Stack, K. M., Farley, K. A., Simon, J. I., Newman, C., et al. (2023). Overview and results from the Mars 2020 Perseverance rover's first science campaign on the Jezero crater floor. *Journal of Geophysical Research: Planets*, 128(6), e2022JE007613. <https://doi.org/10.1029/2022JE007613>
- Temel, O., Senel, C. B., Spiga, A., Murdoch, N., Banfield, D., & Karatekin, O. (2022). Spectral analysis of the Martian atmospheric turbulence: InSight observations. *Geophysical Research Letters*, 49(15), e2022GL099388. <https://doi.org/10.1029/2022GL099388>
- Toledo, D., Gómez, L., Apéstigue, V., Arruego, I., Smith, M., Munguira, A., et al. (2023). Twilight mesospheric clouds in Jezero as observed by MEDA Radiation and Dust Sensor (RDS). *Journal of Geophysical Research: Planets*, 128(7), e2023JE007785. <https://doi.org/10.1029/2023JE007785>
- Vicente-Retortillo, Á., Valero, F., Vázquez, L., & Martínez, G. M. (2015). A model to calculate solar radiation fluxes on the Martian surface. *Journal of Space Weather and Space Climate*, 5, A33. <https://doi.org/10.1051/swsc/2015035>
- Viudez-Moreiras, D., Lemmon, M., Newman, C. E., Guzewich, S., Mischna, M., Gómez-Elvira, J., et al. (2022). Winds at the Mars 2020 landing site: I. Near-surface wind patterns at Jezero Crater. *Journal of Geophysical Research: Planets*, 127(12), e2022JE007522. <https://doi.org/10.1029/2022JE007522>

- Wang, H., Zurek, R. W., & Richardson, M. I. (2005). Relationship between frontal dust storms and transient eddy activity in the northern hemisphere of Mars as observed by Mars Global Surveyor. *Journal of Geophysical Research*, *110*(E7), E07005. <https://doi.org/10.1029/2005JE002423>
- Zurita-Zurita, S., de la Torre Juárez, M., Newman, C. E., Viúdez-Moreiras, D., Kahanpää, H. T., Harri, A.-M., et al. (2022). Mars Surface Pressure Oscillations as precursors of large dust storms reaching Gale. *Journal of Geophysical Research: Planets*, *127*(8), e2021JE007005. <https://doi.org/10.1029/2021JE007005>